Results in Engineering 27 (2025) 105670

Contents lists available at ScienceDirect

Results in Engineering

journal homepage: www.sciencedirect.com/journal/results-in-engineering

A hybrid approach to enhance decision-making in marine structures: Combining sensor data with human perception

Jacopo Bardiani *, Corrado Mazzolatti, Andrea Manes, Claudio Sbarufatti

Department of Mechanical Engineering, Politecnico di Milano, Via G. La Masa 1, 20156 Milano, Italy

ARTICLE INFO

Keywords:
Human perception
Hard/soft information fusion
Structural health monitoring
Ship structures
Extreme loading conditions
Structural integrity
Pattern recognition

ABSTRACT

In modern ships, safety procedures during emergency responses to incidents often rely on a combination of manual human assessments and communication among personnel. However, this approach can introduce inefficiencies, delays, and miscommunication, ultimately compromising the accuracy and timeliness of decision-making. Structural Health Monitoring (SHM) systems provide real-time damage data, but their effectiveness is limited by the complexity and scale of the ship's structure. Moreover, human observation remains crucial, particularly when sensor coverage is incomplete or uncertain. In this paper, we propose a novel probabilistic framework that systematically integrates sensor data, numerical simulations, and human input to enhance real-time decision-making during missions. Unlike traditional approaches, this framework provides a structured method to incorporate human observations into the assessment of structural integrity, allowing a mathematical reduction of uncertainty in the ship's damage state after an incident. By leveraging offline databases of damage morphology and an onboard pattern recognition system, the novel approach improves the accuracy of failure probability (PoF) predictions, demonstrating that human input—when integrated in a structured and quantitative manner—can significantly refine reliability assessments. The results show a substantial reduction in the uncertainty associated with PoF estimation, particularly in high-risk conditions where human assessments play a key role. This integrated approach provides a novel and practical strategy to enhance both operational efficiency and safety in maritime operations.

1. Introduction

As an illustrative example, consider a ship under attack or facing an emergency. In such scenarios, the safety service currently relies on large crews to subjectively assess the ship's condition and respond to incidents following an attack [1]. Key roles include the command-and-control office, the compartment supervisors, and the safety compartments maintenance teams. Specifically, each compartment has an assigned supervisor responsible for supervising the work of the safety maintenance team and for coordinating information with the command-and-control office. The latter is tasked with evaluating the reported damages and making timely decisions on corrective actions to mitigate the impact of the event.

However, the flow of information between these actors is often inefficient. As a result, valuable time is lost, critical details may be miscommunicated, and damage assessments can be inaccurate, leading to delayed or potentially incorrect decisions in hazard containment [2]. While this is just one possible scenario, it exemplifies the broader challenges of coordinating damage assessment, decision-making, and response actions in high-stress environments.

Based on the previous example, the current structural integrity (SI) assessment procedure for ships should be integrated into a more effective framework to address inefficiencies that make decision-making critical and uncertain after an emergency. This framework should optimize processes and improve coordination while preserving the essential role of human judgment [3].

In this context, where both diagnostic and prognostic are key factors, installing sensors throughout the ship's structure can provide significant benefits by means of structural health monitoring (SHM) techniques, which allow for a real-time assessment of the structural health using sensors as strain gauges or optical fibres [4,5]. For these reasons, SHM strategies can be critical in preventing catastrophic consequences, ensuring that necessary actions are taken quickly to mitigate the impact and maintain the integrity of the vessel (i.e. recoverability) [6–10]. For example, in the maritime industry, the use of permanently installed sensors is widespread for acquiring data during missions [11–13], so that once the damage occurs, the strain measured by the sensors will

* Corresponding author at: Department of Mechanical Engineering, Politecnico di Milano, Via G. La Masa 1, 20156 Milano, Italy.
E-mail address: jacopo.bardiani@polimi.it (J. Bardiani).

https://doi.org/10.1016/j.rineng.2025.105670
Received 26 March 2025; Received in revised form 7 June 2025; Accepted 8 June 2025
Available online 8 June 2025

Nomenclature

Symbols

$L_{B.P.}, B, D, T, L$	Containership portion geometry data
$A, B, \alpha, C, m, \dot{\varepsilon}_0, T_{ROOM}, T_M$	Johnson-Cook law parameters
ρ_f, c	Properties of seawater
$P, Q, M_{WV,H}$	Ship operational load
$\boldsymbol{u}, \boldsymbol{v}$	Strain vectors
h	Index for specific strain value in vectors u-v
n	Total number of simulations in database
m	Total number of sub-damage simulations
z	Index for specific structural element beneath removed panels
W_i	Weight based on SSE for the i-th case
τ	Ship transversal section index
σ	Navier stress
$f_s(s)$	Probability density function of stresses
$\mu_{mat}, \sigma_{mat}, \gamma_r$	Probabilistic material properties
w	Number of structural elements requiring human verification
D_q	q-th structural element human report
δ	Number of reports requested from the crew
ω_τ	Weight of τ-th section
E, ν, ρ	Typical naval mild steel mechanical properties
$D_i, \varepsilon_0, \sigma_H, \sigma_{eq}, d\bar{\varepsilon}^p_{eq}, l_e, t_e, \varepsilon_n, k$	RTCL damage model parameters
$M, R, t, t_{detonation}, p(t)$	UNDEX parameters
$F_M, n, C, L_{B.P.}, B, C_b, k_c$	IACS parameters to compute $M_{WV,H}$
k	Strain vectors u-v length
i	Index for database simulation
j	Index for sub-damage simulation
$\boldsymbol{DS}_{ij}$	Damage state ij-th
p	Total number of structural elements beneath removed panels
K_z	Post-damage residual stiffness for the z-th element
θ	Total number of ship transversal sections
M, I_y, z	Parameters for σ
$F_R(s)$	Cumulative distribution function of material's yielding limit
ψ	Number of samples from LHS
q	Index of structural element requiring human verification
$\boldsymbol{DSR}_\delta$	Damage state report vector for δ-th report
H	Shannon entropy

Abbreviations

RUL	Residual useful life
UNDEX	Underwater explosion
NLFE	Non-linear finite element
UQ	Uncertainty quantification
KDSS	Knowledge-based decision support system
SI	Structural integrity
LHS	Latin hypercubic sampling
BCs	Boundary conditions
FBG	Fiber bragg grating
DS	Damage state
CDF	Cumulative distribution function
RTCL	Rice-Tracey and Cockcroft-Latham
SHM	Structural health monitoring
FEM	Finite element method
pdf	Probability density function
DNN	Deep neural network
PoF	Probability of failure
HiFi	High fidelity
ANN	Artificial neural network
MPC	Multi-point constraint
SSE	Sum of squared errors
KDE	Kernel density equation
MSE	Mean squared error
IACS	International association of classification societies

change based on the entity of the damage itself (e.g. damage position and dimension).

Despite the great advantages behind SHM systems, they have evident limitations when applied to ships, which are large and complex structures [14–16]. It is not feasible to install sensors everywhere, meaning there will always be gaps in the ability to accurately understand the location and especially the morphology of damage. The latter information can be crucial not only for assessing SI but also for decision-making, when considering hull damage that can lead to flooding. Furthermore, we have not yet reached the point of having highly efficient automated SHM systems, which means we cannot rely solely on them; thus, human input remains essential not only for maintenance but also for detailed damage reporting and observation [17].

For all the previous reasons, the synergistic integration of information from sensors and human sources (so-called hard/soft information fusion [18]) represents a prominent topic in the current literature, and efforts are underway to develop frameworks that facilitate this integration, with the goal to enhance the ability to perform diagnosis and prognosis (e.g. predict the residual useful life (RUL) [19]) on the ship, to optimize the real-time decision-making process. However, there are at least three non-trivial aspects when trying to acquire damage knowledge through human observation reports [20]. The first is that the ship damage conditions are too complex to judge in scene after emergency due to a great probability of flooding and fire which cause uncertainties in forecast the damage consequences. The second aspect is the limited time available for damage check, meaning that if containment actions are not executed promptly, the ship may become irrecoverable. The third factor involves the inherent uncertainty introduced by the ship's crew during hazardous situations [21,22]. In fact, individuals responsible for damage assessment face significant stress, knowing their actions directly impact the safety of themselves and others. This pressure can impair both judgment and performance [23,24]. Crew members, particularly those handling maintenance or reporting critical information during emergencies, are influenced by performance shaping factors [25], such as the environment, work hours, organizational structure, and available equipment. Additionally, psychological (e.g., stress, distractions) and physiological factors (e.g., fatigue, hunger) further impact their performance [20]. For all the previous reasons, uncertainty quantification (UQ) in SHM is essential both for sensor reading and human knowledge [26,27].

In recent years, the SHM field has seen significant progress, with growing interest in probabilistic and Bayesian approaches to manage uncertainty and improve decision-making in real-time scenarios. Recent works have introduced advanced Bayesian inference techniques, dynamic models, and data fusion strategies that enhance the accuracy and robustness of SHM systems in various engineering applications [28–35]. These contributions highlight the potential of combining sensor data and probabilistic reasoning to enable more informed and timely responses to structural damage.

Previous attempts at fusing hard and soft data, such as those presented in Refs. [1,36], primarily focus on knowledge-based decision support systems (KDSS) that leverage pre-defined logic to combine sensor readings with human expert knowledge. While these systems are effective in reducing damage diagnosis time and providing support

under stressful scenarios (e.g., fire or flooding onboard), they often lack adaptive learning and probabilistic reasoning capabilities, limiting their responsiveness in evolving conditions. Similarly, studies described in Refs. [37,38] investigate multi-sensor fusion architectures that attempt to correlate automated sensor data with human-reported patterns. These approaches help refine observations post hoc but typically treat human input as a static data source, rather than as a dynamic, updateable component of the monitoring system. Moreover, although risk-informed decision-making is gaining attention in SHM (as in the recent framework proposed [39]), current probabilistic models—while powerful—are generally not designed to ingest human observations alongside physical data in real-time feedback loops. As an example, in Ref. [39] a Bayesian network-based structure is used to model uncertainty in damage diagnosis and decision-making. However, the framework operates mainly within the domain of hard data, without addressing the integration of subjective insights or operator observations, which are often crucial in real-world marine applications.

While the previous approaches and attempts show promise in enhancing damage diagnosis and decision-making support, they are often limited by the inability to integrate real-time human insights directly into the system to continuously refine and improve sensor-based information on-board ships [40,41].

In this context, we propose a novel probabilistic framework for ship operations, integrating sensor data, numerical simulations, and human expertise to reduce the uncertainty associated with the probability of failure (PoF) in response to emergency events, like impacts. This approach enhances real-time decision-making, optimizing both operational efficiency and safety by accounting for damage variability and the inherent uncertainty in human judgment.

This work does not focus on advancing reliability modelling itself but rather on developing a comprehensive framework that contextualizes decision-making in naval emergency scenarios. The proposed approach integrates existing reliability assessment methods with real-time data processing and human expertise, providing a structured methodology that can be applied to enhance response strategies and improve overall situational awareness.

In particular, the framework is implemented to a portion of a containership: complex damage induced by underwater threat is initially simulated with high fidelity (HiFi) and then simplified, ensuring that the simplified models still accurately represent the significant effects of the damage. To initially locate the damage, a database of simulated (and simplified) damages created offline is leveraged, and a pattern recognition metric is used to compare strain data from the sensor network on the structure with the data from the damage database. Once this is done, the SI is assessed based on the previous comparison, focusing on different sections of the ship to reconstruct the probability distribution of stresses. This is achieved through the usage of a second offline database that considers a more refined representation of the morphology of the damages, necessary for a correct calculation of a SI parameters and the consequently stress distributions. Considering then a limit state for the material of the structure, the evaluation of the PoF of the structure is performed. According to a PoF's threshold, human knowledge is then inserted in the framework by classical Bayesian probabilistic approach, to reduce the uncertainty related to the computation of PoF, resulting in enhanced on-board decision-making process.

Although this study focuses on an emergency scenario induced by an underwater explosion, the proposed framework is versatile and can be applied to other critical situations, such as collisions or grounding, for structural integrity assessment.

While the framework is primarily intended for application on combatant ships, the limited availability of complete structural models for such vessels led to its implementation on a portion of a containership. This choice does not compromise the reliability of the framework demonstration, as the containership model provides a suitable reference for validating the proposed approach.

The manuscript is organized as follows. The research framework methodology is reported schematically in Section 2. Section 3 focuses on the application of the entire methodology to a real case study, represented by a portion of a containership. All the results are provided in Section 4 and the conclusions of the work and possible future developments are stated in Section 5.

2. Research framework methodology

The proposed framework combining sensors data, FEM simulations and human information is composed by the following steps, graphically schematized in Fig. 1.

The framework is divided into two key nterconnected phases: offline and online. Offline phase refers to all the analyses conducted prior to the mission, ensuring that relevant data are precomputed and readily available for real-time use. These analyses include tasks such as creating damage databases through FEM simulations, and training machine learning models or algorithms. On the other hand, online phase involves real-time calculations during the mission, particularly after an attack inducing structural damage. This phase utilizes precomputed data and information to make informed decisions and support real-time response to the damage scenario.

The key aspects of the diagram in Fig. 1 are described below.

- HiFi simulated "target" damage of an underwater explosion event against the double bottom of a portion of a containership model, inducing hull breakage. An explicit dynamic numerical framework is considered comprehensive of a HiFi representation of the material's failure mode, capturing the realistic damage morphology. This model is also subject to operational loads, and it is used as the first "target" case to test the functionality of the framework in a realistic scenario and to build simplified numerical models.
- A simplified simulated "target" damage model is created by using the extent and distribution of damage from the HiFi simulation as a reference. A simplified approach, as proposed by the Naval Society of Classifications [42], is applied, representing the damage by removing the external panels destroyed by the extreme event, thus creating a simplified version of the HiFi damage. This simplified model serves as an additional "target" case that will be validated in the case study application. This model with simplified damage is assumed to be subjected to operational loads only.
- For the damage localization phase, an offline database, containing simplified damage numerical simulations, is created. This database is composed of FE models with several damage configurations, by varying the removed external panels of the outer bottom.
- A metric for patter recognition is used within the online phase to compare the strain data extracted from a fiber bragg grating (FBG)-based sensor network installed on the "target" model with the strain pattern of each case available in the offline database. The scope of this comparison is to rank the simulated cases in the offline database according with their similarity to the "target" damage, based on strain comparison.
- Sub-damage database morphology aims to create a secondary offline damage database, simulating complex combinations of damaged structural elements based on the most probable cases identified in the first database. Differently from the first database, here the scope is to consider the morphology of the damage in a simplified way, so different combinations of damaged structural elements need to be considered, accounting that following an accident, each structural element involved can have a different residual stiffness state. The sub-damage database can be created by means of different strategies: experience and physics-based approach, Latin Hypercubic Sampling algorithm (LHS) and through a combination of LHS and artificial neural network (ANN).
- A SI assessment is performed analytically in a simplified wat to evaluate the actual ship state (after the damage) with the

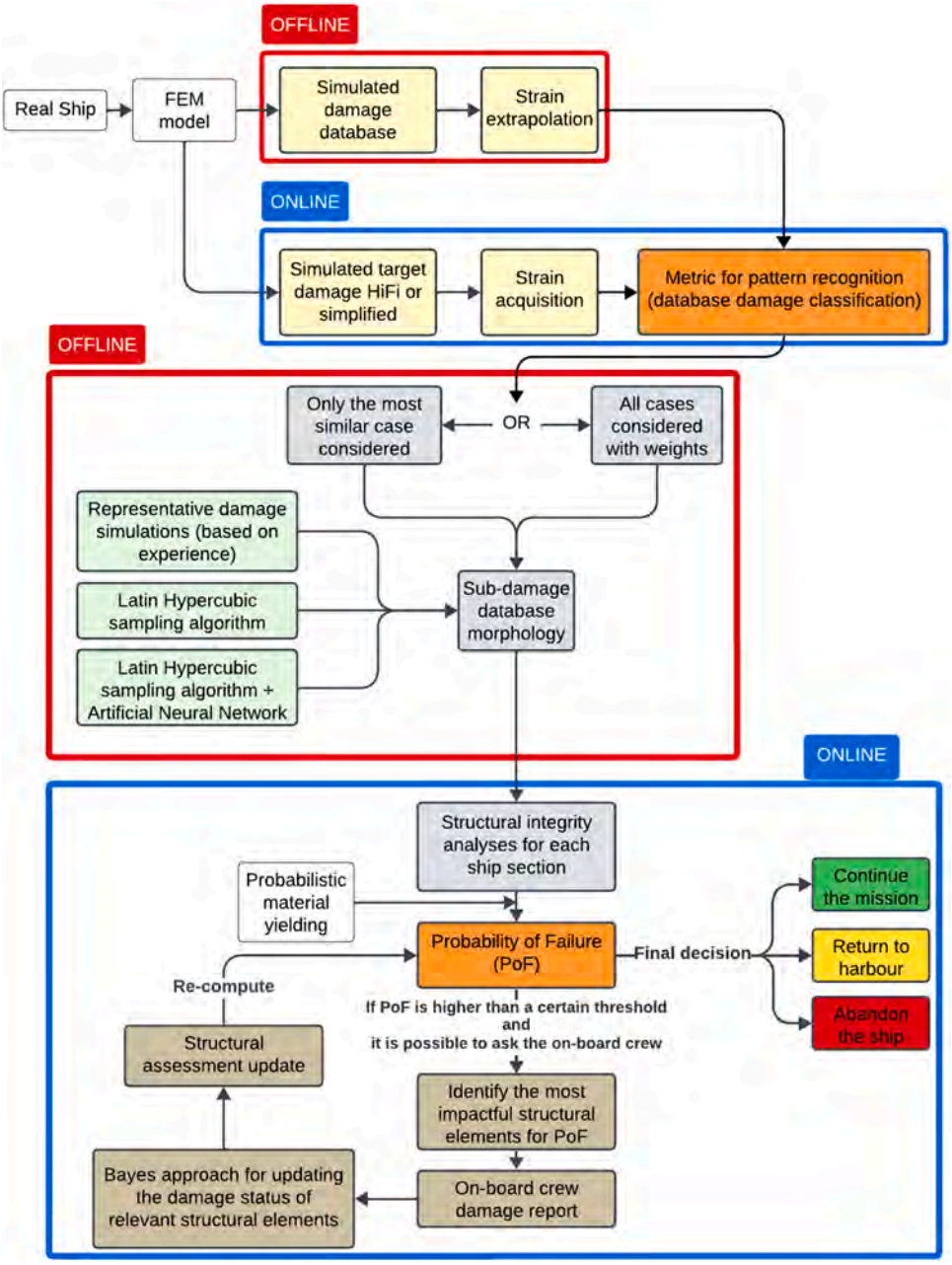

Fig. 1. Workflow chart of the framework implemented in the presented research.

computation of Navier stresses, on several transversal sections of the ship, for each damage combination within the sub-damage database.

- The PoF is then computed to understand, based on the current damage SI available information, how far the actual ship state is from the material yielding limit, which, for a complete analysis, is considered not as a deterministic material property but with uncertainty. Based on the calculated value of PoF and a user-defined threshold, the crew can decide whether to involve human intervention or not.
- If human intervention is needed, the on-board crew knowledge loop is considered. Information about the status of one or several structural elements (considered determinant for the PoF calculation) is requested, considering uncertainty in human's judgment. The information coming from the crew is used to update the PoF and reduce its variability using the Bayesian approach. Human knowledge is integrated to update at posterior the probability of each damage combination presents in the sub-damage database. Considering the damage induced by an underwater explosion, it is assumed that the ship's crew includes a specialized team capable of diving to assess the extent of the damage.

3. Case study

3.1. Simulated "target" damage model

The simulated target damage model represents the model that mimics the behaviour of the ship when subjected to the extreme event of an underwater explosion. Conducting an experimental campaign to analyse such damage would require deliberately subjecting a vessel to an explosive event, a process that is not only highly complex and costly but also logistically unfeasible. Additionally, there is a lack of literature available datasets containing detailed structural response data for such scenarios. For these reasons, our study relies on numerical simulations to generate the necessary input. Two versions of this model, differing in the

level of approximation, are used in the framework and are described in detail in Sections 3.1.1 and 3.1.2. Since the goal of this study is to demonstrate the feasibility of the proposed framework rather than to replicate real-world sensor outputs precisely, the use of FEM simulations as a starting point is justified within the scope of this work

3.1.1. HiFi simulated "target" damage model of an underwater explosion (UNDEX)

This section contains a detailed description of the FEM model of the selected containership portion in paragraph 3.1.1.1, followed by an explanation of the non-contact UNDEX event in paragraph 3.1.1.2. Finally, operational loads are applied to the damaged model to simulate realistic conditions, as explained in paragraph 3.1.1.3.

3.1.1.1. Containership portion FE model. The geometry considered for the demonstration of the proposed framework corresponds to part of the midship region of a containership with length $L_{B.P.} = 353.0[m]$, breadth $B = 51.0[m]$, depth $D = 29.9[m]$ and designed draught $T = 14.5[m]$. The length of the ship section considered is $L = 27.0[m]$. Fig. 2 contains a schematic representation of the employed case study including the geometry as well as the applied loads.

In the interest of brevity, the reader is referred to [43,44] for detailed structural information. The non-linear finite element (NLFE) calculation of the present paragraph was made in ABAQUS/Explicit version 6.23 [45,46]. In Fig. 2, the compartment bulkheads located at the ends of the ship's portion are not shown for simplicity. The structural numerical model is composed of 1172,058 4-node quadrilateral shell elements with full integration (Fig. 3(a)). The average mesh size is 100 mm, while no refinement strategy has been adopted. The mesh size was determined after performing a mesh convergence process, to ensure that both displacements and stresses are accurately captured in the most important locations.

Typical naval mild steel properties are used, namely $E = 209[MPa]$, Poisson's ratio $\upsilon = 0.3[-]$ and density $\rho = 7850[kg/m^3]$ [47,48]. The plastic behaviour of the material is modelled using the Johnson-Cook law, with the parameters shown in Table 1 [49,50], where A represents yield stress, B is the strain hardening coefficient, α represents the hardening index, C is the rate hardening coefficient, m is the temperature softening coefficient, $\dot{\varepsilon}_0$ is the reference strain rate, T_{ROOM} is the room temperature and finally T_M is the melting temperature.

Structural damage behaviour is considered, using the Rice-Tracey and Cockcroft-Latham (RTCL) damage model [51]. It is a specific ductile failure criterion based on the combination of two models for predicting ductile failure: the Cockcroft-Latham criterion, which addresses ductile shear fracture or more broadly the low triaxialities range, and the Rice-Tracey criterion [52], which is based on void growth and coalescence and is more suitable for high triaxialities. It consists of the following formulation:

$$D_i = \frac{1}{\varepsilon_0} \cdot \int f\left(\frac{\sigma_H}{\sigma_{eq}}\right)_{RTCL} d\varepsilon_{eq}^p \tag{1}$$

In which:

$$f\left(\frac{\sigma_H}{\sigma_{eq}}\right)_{RTCL} = \begin{cases} 0, \text{ for } \dfrac{\sigma_H}{\sigma_{eq}} \le -\dfrac{1}{3} \\ 2 \cdot \dfrac{1 + \dfrac{\sigma_H}{\sigma_{eq}} \cdot \sqrt{12 - 27 \cdot \left(\frac{\sigma_H}{\sigma_{eq}}\right)^2}}{3 \cdot \dfrac{\sigma_H}{\sigma_{eq}} + \sqrt{12 - 27 \cdot \left(\frac{\sigma_H}{\sigma_{eq}}\right)^2}}, \text{ for } -\dfrac{1}{3} < \dfrac{\sigma_H}{\sigma_{eq}} < \dfrac{1}{3} \\ \dfrac{1}{1.65} \cdot e^{\frac{3}{2}\frac{\sigma_H}{\sigma_{eq}}}, \text{ for } \dfrac{\sigma_H}{\sigma_{eq}} \ge \dfrac{1}{3} \end{cases} \tag{2}$$

More specifically, D_i is the normalized ductile failure damage indicator, ε_0 represents the damage strain parameter, σ_H is the hydrostatic stress, σ_{eq} is the equivalent von Mises stress, while $d\varepsilon_{eq}^p$ represents the effective plastic strain increment. The RTCL damage model is sensitive to the size of the mesh; for this reason, the following equation has been proposed to determine the parameter ε_0, which is the only parameter necessary to implement the criterion [51]:

$$\varepsilon_0\left(\frac{t_e}{l_e}\right) = k + (\varepsilon_n - k) \cdot \frac{t_e}{l_e} \tag{3}$$

Where l_e is the mesh element size, t_e is the structural element size (thickness of the bottom plate, to have the lowest value of t_e/l_e), ε_n is the failure strain at $t_e/l_e = 1$ for uniaxial strain (taken from [51]) and k is the power law coefficient (Table 2).

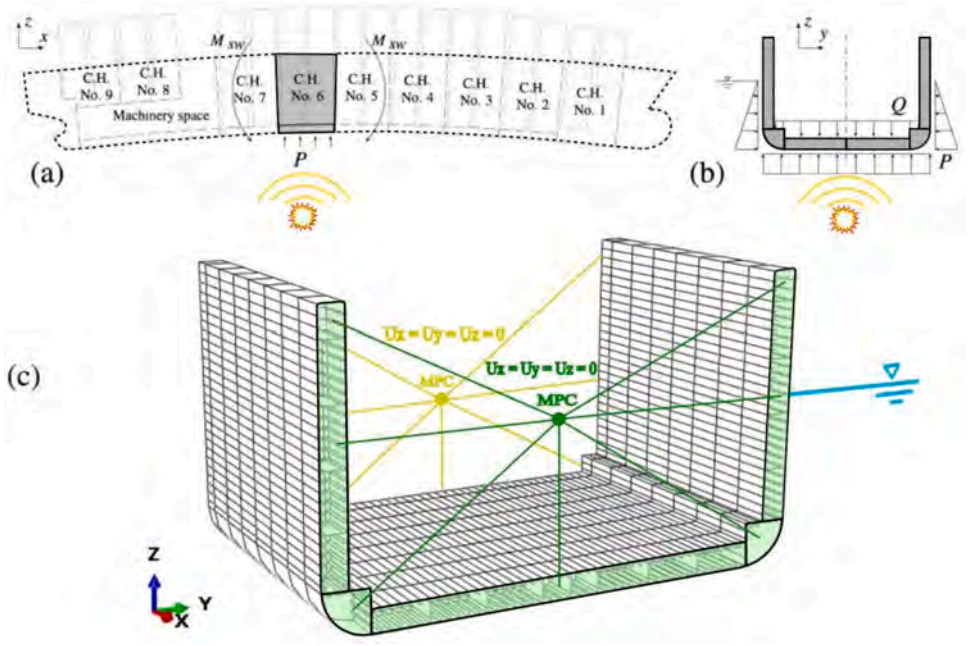

Fig. 2. 3D schematic representation of the benchmark case study under investigation (adapted from [43]). Bulkheads are not shown for visualization purposes.

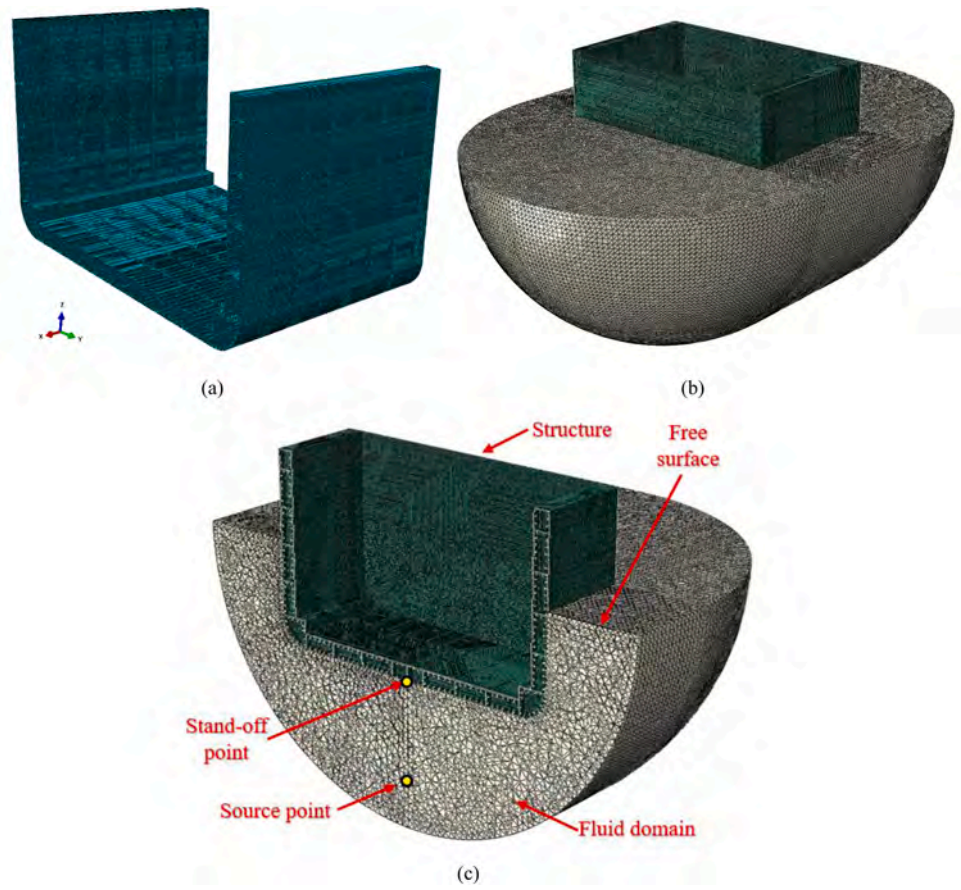

Fig. 3. (a) Mesh of the structural model (without bulkheads), (b) global FEM model of the ship portion surrounded by the external fluid, and (c) vertical section of the FEM model for visualization purposes.

According to the RTCL model, if during the analysis some finite elements reach a damage $D_i = 1$ (i.e. the failure criterion value), they will be considered as totally damaged and removed from the calculation.

The analysis in ABAQUS/Explicit consists of two steps: in the first one, the structure is subjected to a non-contact UNDEX event considering a TNT charge; in the second, the damaged structure is subjected to operational loads. The first step duration is set to allow for structure stabilization after the UNDEX load. For both steps, the same boundary conditions (BCs) are used for simplicity (see Fig. 2).

3.1.1.2. Non-contact UNDEX step. The characteristics of the UNDEX event have been considered as known and deterministic. To model this event, the coupled acoustic-structural analysis strategy in ABAQUS is employed [53,54]. The core of this approach is to divide the UNDEX impact process into two phases: one prior to the onset of loading on the structure and the other following it. The simulation focuses solely on the second phase, neglecting the propagation of the incident wave from the UNDEX source to the structure. To impose the incident wave loading on the structure, the water domain undergoes an acoustic-field initialization at the start of the numerical analysis [55]. By excluding the modelling of incident wave propagation, the cut-off strategy becomes more efficient and, from a structural analysis standpoint, appears more practical. However, this efficiency comes at the expense of accurately modelling the incident wave loading on the structure. In a transient UNDEX analysis using the coupled acoustic-structural approach, a reference point (named stand-off point) from the explosion source is defined to prescribe the time history of pulse loading (see Fig. 3(c)). Using this pulse history and the spatial relationship between the reference point and the source one, the acoustic-field initialization and its subsequent evolution are determined, along with the incident wave loading on the structure [54]. For a comprehensive overview of the approach and the governing equations of this approach, refer to [54].

Fig. 3(b) shows the numerical model, comprehensive of the model of the ship section surrounded by the fluid. The water domain is represented by 1078,561 fluid elements AC3D8R (8-node acoustic brick elements) with appropriate base size, given the properties of seawater. In particular, the bulk modulus is $\rho_f \cdot c^2 = 2.03[GPa]$, and the mass density is $\rho_f = 1024\left[kg/m^3\right]$. The velocity of sound in water is assumed to be $c = 1500[m/s]$. The total wave formulation is used in the analysis to

Table 2
Identification of the parameters of the steel used within the Rice-Tracey and Cockcroft -Latham criteria (RTCL).

$l_e[mm]$	$t_e[mm]$	$\frac{t_e}{l_e}[-]$	$k[-]$	$\varepsilon_n[-]$	$\varepsilon_0[-]$
100	20	0.2	0.20	0.67	0.294

Table 1
Material parameter used in the numerical simulation.

$A[MPa]$	$B[MPa]$	$\alpha[-]$	$C[-]$	$\dot{\varepsilon_0}\,[s^{-1}]$	$m[-]$	$T_{ROOM}[K]$	$T_M[K]$	*Ref.*
314.0	600.00	0.210	0.015	1.0	0.60	293	1800	[49,50]

capture the effects of the cavitation [56].

To determine an appropriate fluid domain thickness and the maximum allowable element length for it, a modal analysis of the containership structure was performed, and it was assumed that the global first-mode natural frequency of the structure should be adequate for estimating the maximum allowable fluid element length [54,57]. About the fluid domain thickness (the radius of the water domain), the authors followed the considerations reported in [54] as guidelines. The total horizontal length of the fluid model with the spherical ends was 97 m and the vertical length of the fluid domain (starting from the free surface) was 35 m. The outer boundaries of the external fluid are represented by semi-cylindrical surfaces and spherical ends with the appropriate non-reflecting BCs.

The fluid-structure interaction between the water and the structure is defined at their common wetted interface with a surface-based tie constraint. The dynamic acoustic pressure at the upper surface of the water is set to zero to enforce a free surface BC (still water).

In this case, a TNT charge weighing $M = 100[kg]$ is detonated below the outer bottom of the structural model with a stand-off distance $R = 10.0[m]$, to represent a real attack's scenario. The reference point for inputting the loading history is positioned exactly on the geometrical centre of the outer bottom surface (Fig. 3(c)). The effects of gas bubble dynamics have been intentionally neglected in this study for the sake of simplicity.

Analysis time was set to $t = 0.050[s]$ to reach the maximum damage that occurs on the structure, while the time of detonation is $t_{detonation} = 0.0[s]$. The decay stage of the numerical loading history at the reference point (Fig. 3(c)), $p(t)$, is compared to the one approximated by Cole's formulations [58], showing a good agreement (not reported here for simplicity).

3.1.1.3. Operational loads application step. In the second step of the analysis (where the structural deformations and damage patterns have stabilized), the operational loads reach the total magnitude very slowly to approach the conditions of quasi-static application of loads [59]. For this case, the total time is set to 0.5 s. The applied loads consist first of uniform hydrostatic pressure P on the outer bottom and side plates, which presents a maximum value equal to $129.7[kPa]$. The second action is represented by the cargo weights, Q, with magnitude equal to $71.41[kN/m]$. The latter is expressed as a line load applied on the lines where the inner bottom meets the transverse webs and longitudinal girders. In addition, a third bending action related to the longitudinal primary stress response of the vessel is considered and applied to the multi point constraints (MPCs) (type beam [60]) of Fig. 2, through the implementation of the formulation proposed by International Association of Classification Societies (IACS) [61]. The equations used here for the hogging load condition is the following:

$$M_{WV,H} = +190 \cdot F_M \cdot n \cdot C \cdot L_{B.P.}{}^2 \cdot B \cdot C_B \cdot 10^{-3} = 6.3 \cdot 10^6 \ [kNm] \quad (4)$$

Where F_M is the factor of distribution of the bending moment over the length of the ship and can be obtained from tables, n is the navigation constant, C is the wave parameter, $L_{B.P.}$ is the sizing length of the vessel in meter, B is the maximum width out of the frame amidships while C_B is the total fineness coefficient of the vessel, calculated out of planking, therefore including the factor $k_C = 1.006$. No information about the precise values is reported here for simplicity, since IACS formulations are well-known in the field of marine engineering design. Finally, the model is also subjected to self-weight.

3.1.2. Simplified simulated "target" damage model

The previous HiFi numerical model is complex and computationally expensive, and it is only used in this framework as a target simulation of a potential real damage morphology, replacing the experimental test which is not yet available. For these reasons, a simplified but representative model of the actual damage was also developed. This simplified model, together with the previous one, were used to represent the target damage for the demonstration of the entire framework.

Starting from the simulation performed in the previous paragraph, the damage is approximated by removing the outer bottom plates destroyed due to the UNDEX event. The authors point out that this approach, albeit with some different features, is the one proposed by some societies of classification to consider a threat damage on the hull. For instance, Lloyd's Register proposes the definition of a cylinder of appropriate size (to be positioned in the more unfavourable position for the structure) that cuts part of the hull inducing a reduction in the SI [42]. The damaged model is then simulated in a static environment, with the same loads and BCs described in the second step of the analysis of the previous paragraph. In this approach, the definition of damage is certainly a great simplification, and pretend to mimic the effect of the damage on the structure only in a phenomenological way. The simplified target damage model considered for the implementation of the framework is shown in Fig. 4.

Finally, the authors demonstrated that removing the outer bottom planking is crucial for achieving the desired strain field variation, ensuring accurate damage localization without the need to remove additional structural elements such as girders, floors, or stiffeners.

3.2. Damage localization through a pattern recognition metric

3.2.1. Sensor network selection

The selection and placement of the sensor network is crucial for capturing accurate strain measurements after structural damage. Given the large dimensions of the containership model, the most effective and practical solution is to implement a FBG-based sensor network [11,62]. Fibre optic cables can be strategically attached to the ship's structure with a proper pattern, allowing extensive coverage of critical areas with an interconnected network of fibres. This flexibility enables monitoring of large portions of the ship, including the hull, decks, bulkheads and other essential structural elements, without the need for multiple individual sensors [62,63]. As depicted in Fig. 5(a), the FBG-based sensor network used in this case study is positioned on the inner plating to avoid exposure to seawater. By focusing the sensor network on critical areas rather than covering the entire structure, complexity and costs are reduced. This approach prevents data overload and optimizes the system's performance in the early stages of damage classification, making it both efficient and applicable to full-scale structures. The present sensor network has already been utilized by the same authors in [7], demonstrating its effectiveness in similar applications.

3.2.2. Database creation (offline phase)

The creation of a database is an essential step in enabling the localization of the damage on the ship's structure. This database was made with simplified damage models according to the description made in Section 3.1.2. The purpose of this database is allowing the comparison of strain responses between the structure with target damage (whether from the HiFi or the simplified model) and the simulated damages in the

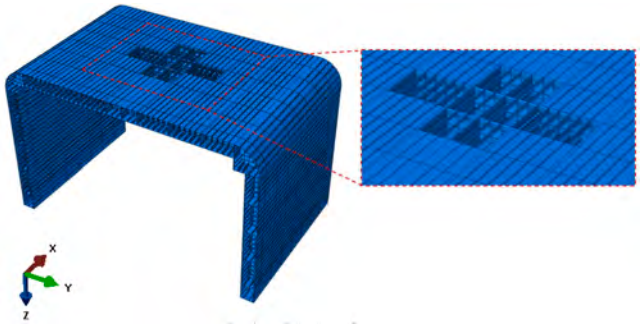

Fig. 4. Visualization of the simplified target damage model.

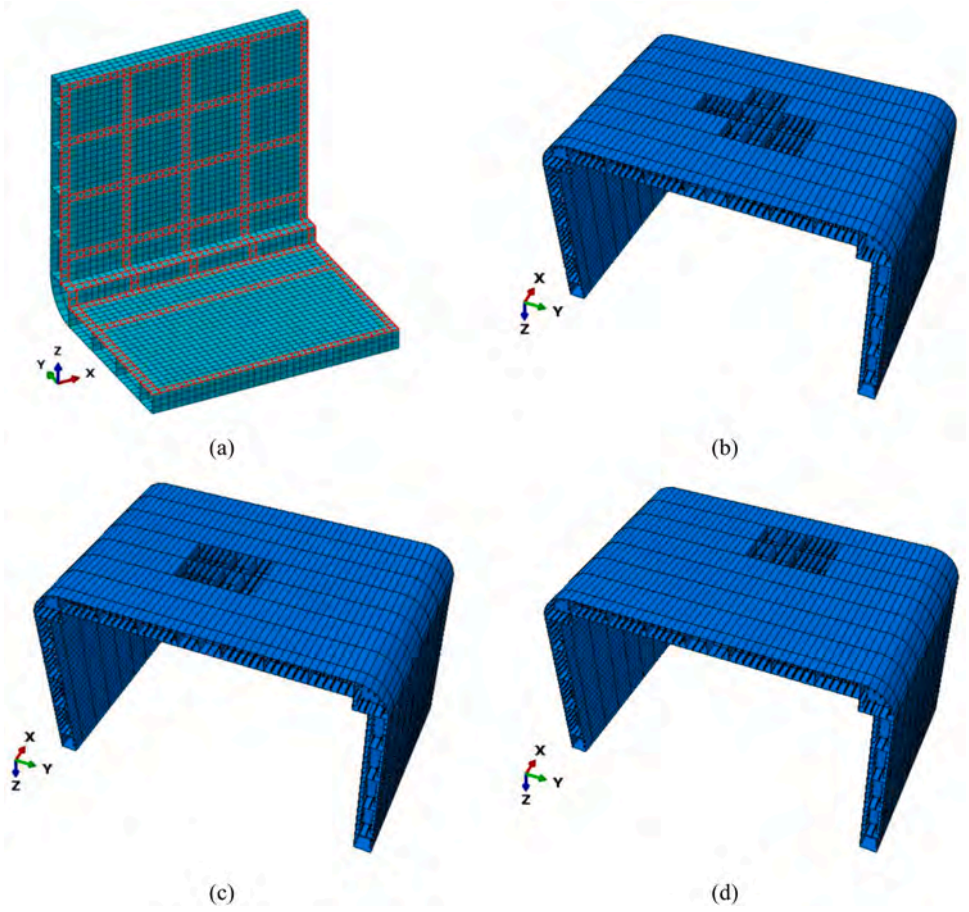

Fig. 5. (a) Representation of the FBG-based sensor network used (only half of the model). (b), (c) and (d): visualization of three different FE models within the offline database, with different damage locations.

offline database, evaluating their similarity for an accurate damage localization. In the present case, for demonstration purposes, only three combinations of damage location within the dataset were considered (Fig. 5(b), (c) and (d)). Within the database, the strain associated to each case serves as the feature for the damage localization process, based on the pattern recognition technique discussed in Paragraph 3.2.3.

From this point onward, the case represented in Fig. 5(b), (c) and (d) are indexed as Case *I*, Case *II*, and Case *III* respectively.

3.2.3. Metric for pattern recognition

Once the offline database is established and all strain data from the sensor networks have been stored, the next step involves acquiring real-time strain data during a mission and comparing them with the database. Here, the strain data from the database are compared with the HiFi and simplified target damages, as outlined in previous sections. It is important to highlight that strain data from FEM simulations differ from real-world sensor network strains, where disturbances such as temperature fluctuations, vibrations from the ship machinery, electrical noise often affect the measurements. FEM models, by contrast, generate smoother, idealized data without these noise factors. In cases of noisy data, the Mahalanobis distance is an ideal mathematical metric for comparing strain vectors, as it accounts for correlations between variables using the covariance matrix, making it ideal for data comparison where non-isotropic noise is present [64]. However, since this study focuses solely on strain data derived from FEM simulations (since data from experimental test are not yet available) noise is not present and the most straightforward and suitable mathematical metric for strain vectors comparison is the sum of squared errors (SSE), also known as Euclidean distance. Given two strain vectors $\boldsymbol{u}$ and $\boldsymbol{v}$ of length k, the SSE is given by the formula:

$$SSE = \sqrt{\sum_{h=1}^{k} (u_h - v_h)^2} \tag{5}$$

The use of the SSE as the primary metric is sufficient in the current case study to efficiently demonstrate the core principles of the framework. Additionally, SSE serves as a solid foundation that can be expanded upon the future work, where the framework needs to address more complex scenarios. For each SSE_i value, a weight W_i is derived by $1/SSE_i$ for the i-th case in the offline database. This means that a low SSE, which indicates a high similarity between the simulated damage strains (within the database) and the target damage strains, corresponds to a high weight W_i. Higher weights indicate greater similarity and thus higher importance for that specific case within the offline database.

Once the weight values are calculated, two approaches can be followed:

- Single damage selection: consider only the simulated damage (within the database) with the highest weight, as it is the most likely.
- Weighted analysis: consider all cases (or a group of them) within the database, rescaling each with its associated weight.

The second approach is more comprehensive, and it is the one followed in the present investigation, as it provides a more detailed and complete representation of the actual damage scenario.

3.3. Sub-damage database creation

Each case in the first database can exhibit various damage morphologies. Therefore, a second database is needed to properly account for the damage in the subsequent SI analyses. Prior to this, the definition of the damage state vector is provided.

3.3.1. Definition of the damage state

For each case presented in the database of Section 3.2.2 (see Fig. 5), identified by the subscript i (with $i = 1,...n$), a series of m sub-cases are considered, which constitute the offline sub-damage database. To identify a specific sub-case for a given case i, the subscript j is used, with $j = 1,...,m$. The damage state vector DS_{ij} is a defined as follows:

$$DS_{ij} = \{K_z | z = 1,...,p\} \tag{6}$$

Where p represents the total number of structural elements beneath the removed panels, and K_z is the percentage of residual stiffness of the z-th structural element beneath the removed panels, including components such as girders, floors, and group of stiffeners (note that since singular stiffeners have a negligible influence on the SI, to reduce the computational cost they have been considered in groups, such that nearby stiffeners are assumed with the same post-damage residual stiffness).

The value of K_z can vary according to the following discrete set (for simplicity):

$$K_z \in \{100\%, 75\%, 50\%, 25\%, 0\%\} \tag{7}$$

These values represent the percentage of the remaining stiffness of each structural element, corresponding to different levels of stiffness retention or loss (for example, 100% indicates that the element retains its full original stiffness, while 0% means that the element has completely lost its stiffness and is no longer able to transfer loads).

For each specific case in the database described in Section 3.2.2, multiple damage states DS_{ij} are generated. Given the complexity of the structure, which consist of many structural elements, each affected by damage (being in one of five possible residual stiffness states identified by K_z), the offline sub-damage database is significantly larger. As an example, if in the damage case i (Fig. 5) there are 10 structural elements beneath the removed panels (girders, floors, etc.), each with 5 possible residual stiffness states K_z, the total number of combinations for the DS_{ij} vector is given by 5^{10}, resulting in $9,765,625$ possible configurations. Given the vast number of possible damage combinations, it is essential to implement strategies to reduce both computational cost and time, while ensuring the sub-damage database effectively captures the full range of damage state variability. To this aim, potential strategies are discussed in the following sections.

3.3.2. Experience-based considerations

The first method for creating the offline sub-damage database relies on the experience of the ship's crew, based on historical damage data from past underwater explosion events. In this way, the number of structural elements damaged combinations can be reduced, since it becomes possible to focus on cases with the structural elements most likely to fail. This allows for the exclusion of unlikely damage scenarios, thereby simplifying the database and minimizing the computational demand. However, the major limitation is that these considerations are based on crew experience and historical data, which may be incomplete, incorrect, or unavailable, potentially affecting the comprehensiveness of the final assessment. For this reason, other alternatives are evaluated.

3.3.3. Latin-hypercubic sampling

To improve the phase of defining the DS_{ij} configurations, LHS technique was implemented. This method enables efficient sampling of the damage states without requiring an exhaustive simulation of all possible combinations [65–67], which would be computationally prohibitive given the high number of structural elements. LHS ensures uniform sampling across the multi-dimensional space defined by the structural elements damage states, represented by the variable K_z. For the sake of completeness, the procedure for applying the LHS technique to discrete variables is outlined in the following steps:

- Domain partition: the range $[0,1]$ is a numerical interval, which is partitioned into ψ equal sub-intervals for each structural element, where ψ represents the number of desired samples.
- Sampling: a random point is selected from each interval, ensuring uniform distribution.
- Random permutation: the samples from each structural element are randomly combined to form ψ unique damage scenarios, ensuring that each element's sample appears exactly once in each combination.
- Discretization of damage states: the continuous samples are then mapped to discrete damage states identified by the variable K_z based on predefined ranges within the interval $[0,1]$ (as defined by the authors).
  - $0 \leq x < 0.2$ correspond to 0% stiffness (element completely broken).
  - $0.2 \leq x < 0.4$ correspond to 25% stiffness.
  - $0.4 \leq x < 0.6$ correspond to 50% stiffness.
  - $0.6 \leq x < 0.8$ correspond to 75% stiffness.
  - $0.8 \leq x \leq 1$ correspond to 100% stiffness (element completely undamaged).

This method guarantees a broad and uniform coverage of the damage space with a limited number of simulations, ensuring efficient exploration of possible damage state configurations while maintaining computational feasibility. In this case study, $1,000$ unique damage state combinations were generated (so ψ is equal to $1,000$). After validation tests with $10,000$ and $100,000$ simulations, it was determined that increasing the number of simulations beyond $1,000$ provided marginal improvements with respect on the computed PoF (refer to Section 3.5 for a detailed PoF explanation), confirming that $1,000$ samples was sufficient to cover the variability domain.

3.3.4. Latin hypercubic sampling and artificial neural network

As shown, given the high number of possible damage state combinations, analysing all of them through direct computation can be computationally prohibitive. Adopting a surrogate model, such as an ANN, is therefore a valid and effective strategy to evaluate the structural response across a wide range of scenarios. In the present study, a Deep Neural Network (DNN) [68] has been implemented in the MATLAB environment to predict the SI parameter for any new damage configuration, based on a training dataset generated via LHS, consisting of 1000 representative damage states. Specifically, a single DNN takes a specific damage state combination DS_{ij} as input and predicts the SI parameter corresponding to the maximum Navier stress (see next section for more details).

The architecture consists of one input layer (with dimensionality equal to the number of rows inside the damage state combination), two hidden layers with both 10 neurons, and one output neuron providing a continuous SI value (Navier stress). All nodes in the DNN employed the ReLU activation function. Training was performed using the Adam optimizer, and the mean squared error (MSE) loss function was used to quantify the difference between predicted and target SI values. An 80/20 train-validation split was adopted, and metrics were monitored during the training process. An early stopping criterion was implemented: if the validation loss did not improve for 100 consecutive epochs, training was terminated, and the model weights were reverted to those corresponding to the epoch with the best validation performance within the last 100 epochs. The final values achieved for the loss function were MSE equal to 0.0011, 0.0015, and 0.0018 for the training, validation and test, respectively. The previous results confirm the

model's good generalization capabilities and the absence of significant overfitting. Fig. 6 shows the loss evolution during the training process for both the training and validation sets, highlighting the convergence behaviour and the effectiveness of the early stopping criterion in preventing overtraining. Furthermore, to assess the robustness of the surrogate beyond the LHS-derived dataset, the trained DNN was tested against additional 500 damage state combinations not included in the initial 1000-sample pool. The results confirmed the model's ability to generalize effectively to unseen configurations, maintaining low prediction errors and stable performance. This supports the applicability of the DNN-based surrogate for real-time SI estimation across a broad range of possible damage scenarios.

In practical scenarios, the structural variability along the hull implies that a dedicated DNN should be trained for each relevant transverse section of the ship, allowing the framework to account for local differences in geometry, stiffness distribution, and vulnerability to damage.

3.4. Structural integrity assessment

The SI of naval vessel is a critical factor in ensuring their operational safety and performance. The primary aspect for assessing the containership SI is understanding how well the longitudinal elements can withstand the longitudinal bending moment on the vertical plane. This is of fundamental importance in both still water and wave conditions, where the distribution of weight and buoyancy leads to significant bending stresses on the hull. In naval architecture, the ability of a ship's structure to resist these longitudinal bending moments is evaluated by analysing the cross-sectional strength of the hull girder. Classifications societies provide guidelines for evaluating the ultimate longitudinal strength of ships [42]. These guidelines emphasize the importance of analysing how the damage impacts the load-bearing capacity of the ship particularly by removing the structural elements that no longer contributes to the hull's longitudinal strength and evaluate the change in the inertia of the damaged transversal ship section. The inertia variation is directly associated with the stress variation calculated on the transversal ship section using the simple beam theory, derived from the thin-walled beam theory based on the assumption of plane section.

Despite the availability of more advanced theories for assessing structural collapse, considering also local evaluations, the framework employs a simplified approach based on beam theory and the yielding criterion, as specified in Refs. [69,70]. Specifically, the stress σ calculated using Navier's formula has been adopted as a parameter for assessing the SI, calculated as:

$$\sigma = \frac{M}{I_y} \cdot z \ [MPa] \tag{8}$$

Where M is the transversal bending moment acing on the cross-section (equal to $M_{WV,H}$), I_y is the moment of inertia on the neural axis, and z is the distance from the calculation point to the neutral axis. By evaluating the Navier stresses across some representative cross sections of the damaged ship, it is possible to quantify how the SI has been compromised due to the occurred damage.

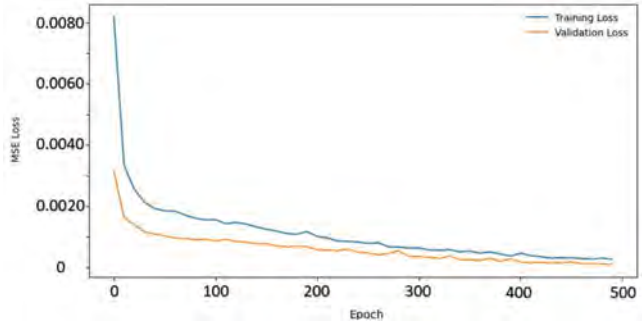

Fig. 6. Training and validation loss curves showing convergence of the DNN model.

Two important clarifications must be made regarding the assumptions and methodology used in this study. First, Eq. (8) was used to compute the maximum stresses analytically, avoiding the impractically large number of FEM simulations that would have been required to populate the database. However, the maximum stress values within the section can still be obtained through FEM analysis if needed. Second, in our model, the material is assumed to be homogeneous. For non-homogeneous materials, the modulus of elasticity would no longer remain constant across the section. Instead, an equivalent elastic modulus should be determined, considering the spatial variation of material properties. This adjustment ensures that the stresses computed using Navier's formula properly reflect the heterogeneous nature of the section.

3.5. Probability of failure

3.5.1. Calculation

To compute the global PoF of the containership, the stress distribution and PoF are both evaluated across several cross-sectional areas. Specifically, the portion of the ship under investigation has been divided into seven transverse sections, as illustrated in Fig. 7. For each of these seven sections, stresses and the consequently PoFs are calculated. Then, having the PoF values for each section, a unique PoF_{global} for the entire model is computed. Initially, the histograms regarding the distribution of stresses have been generated for each cross-section. These stress values are obtained from the offline sub-damage database, and each of them is weighted according to its similarity to the real damage, as derived from the first strain comparison, meaning that the frequencies in the histogram reflect these weights.

Based on the histograms, they are converted into a continuous probability distribution through the kernel density function (KDF) [71], ensuring a good representation of the distribution. The stress distributions need to be compared with the material's yield stress to compute the PoF. Based on the information reported in [72], the material yield stress is modelled with a Gaussian distribution with a mean value μ_{mat} equal to 314 $[MPa]$ and a standard deviation σ_{mat} equal to 4 $[MPa]$. Additionally, a safety factor γ_r has been considered covering material, geometric and strength prediction uncertainties. Referring to the IACS regulations, as stated in the Common Structural Rules for Bulk Carriers and Oil Tankers manual [61], γ_r should be equal to 1.4, but here it was increased to 2 to consider the fact that, as stated in 3.1.1.3, the bending load, due to the lack of data, is approximated by an empirical formula.

To calculate the PoF of each cross-section, the stress distributions are compared with the distribution of the material yield stress for each of the seven cross-sections. The goal is to determine the probability that the computed stress exceeds the yielding threshold. Mathematically, this expresses as [73]:

$$PoF = P(\sigma > R) \tag{9}$$

Where σ is the stress experienced by the structure and R is the material yielding limit.

The calculation of the probability of failure involves the integration of the probability density function (pdf) of stress and the cumulative distribution function (CDF) of the yielding limit. The CDF of the yielding limit provides the probability that the material will yield at a given σ value, thus the overall probability of failure for each transversal section is calculated as [74,75]:

$$PoF = \int_{-\infty}^{+\infty} f_s(s) \cdot F_R(s) ds \tag{10}$$

Where $f_s(s)$ is the probability density function of stresses obtained through the KDF and $F_R(s)$ is the cumulative distribution function of the material's yielding limit. This integral provides the overall PoF for the

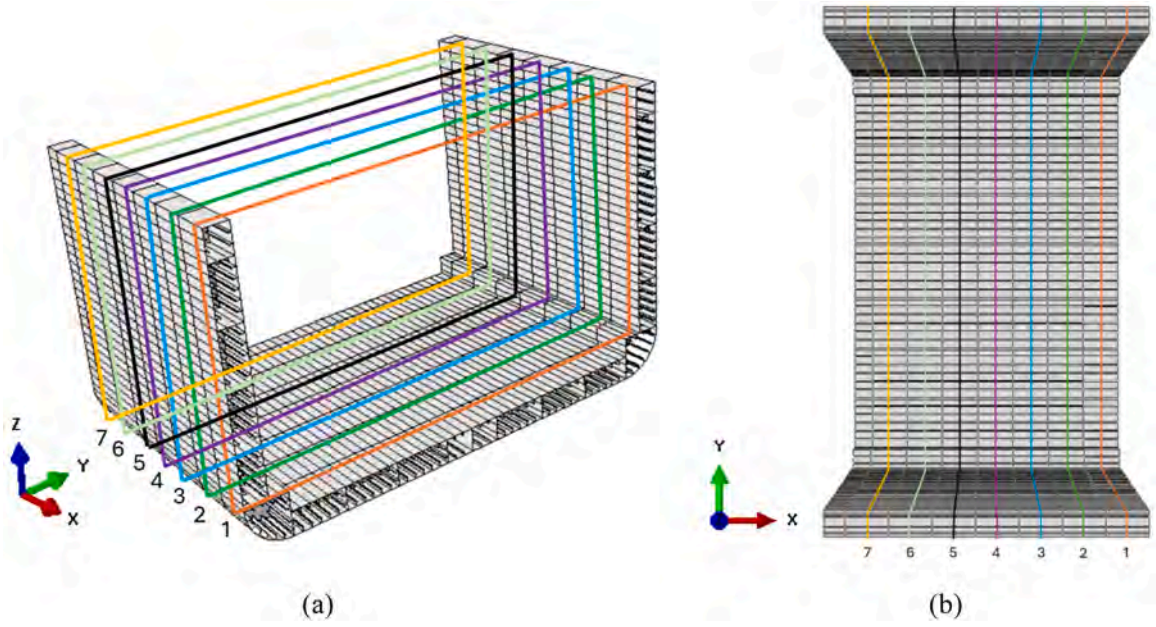

Fig. 7. Visualization of the transversal sections considered for the SI assessment with different views.

cross-section, reflecting the likelihood that the stress values will exceed the material's yielding stress. The value of PoF_{global} was then determined by combining the PoF of each individual section of the structure. Each section has its own PoF, which reflects the likelihood of failure within that section based on stress and other factors like material properties or load conditions. To calculate the global *PoF*, it was assumed that the failure of each section is independent from the others (for simplicity). The formula for combining independent failure probabilities, taken from [75], is as follows:

$$PoF_{global} = 1 - \prod_{\tau=1}^{\theta} (1 - PoF_{\tau}) \tag{11}$$

Where θ is the number of considered transversal sections (which is equal to seven in this case), and PoF_{τ} is the *PoF* of the τ-th section.

3.5.2. Threshold for human perception triggering

After having computed the PoF for each transversal section and PoF_{global}, the latter value must be analysed to determine which is the optimal action to undertake for the mission safety.

Threshold selection within this risk-based decision-making framework is a key point. As noted in the literature, this value can vary significantly depending on ship type, mission profile, risk tolerance policies, and classification rules. For instance, higher tolerance may be accepted in military or exploratory vessels where operational continuity can outweigh conservative safety margins, while much lower thresholds (e.g., PoF $< 10^{-4}$ or even 10^{-9}) are enforced during the design stage of commercial vessels such as containerships or oil tankers [42,76].

Importantly, recent studies in the maritime field have also acknowledged the use of explicit PoF thresholds when assessing residual strength after damage. In Ref. [77], a Bayesian network is used to estimate PoF in damaged ship hulls, proposing decision-making schemes that are based on thresholds derived from structural response statistics. Similarly, the work proposed in Ref. [76] proposed strength-based acceptability criteria for post-damage ship hull integrity, highlighting how practical thresholds depend on the desired residual load-carrying capacity and are scenario-specific.

Additionally, the work proposed in Ref. [78] offers a useful perspective. Although their focus is primarily on tankers during the design phase, they investigate how residual strength reductions and failure probabilities change under multiple damage scenarios. While a precise universal threshold is not defined, their approach shows that post-damage reliability assessment is becoming an increasingly accepted tool, with failure probability being an integral metric for informing structural decision-making.

For the demonstration of the present framework, the threshold for human triggering was set to activate when the PoF_{global} exceeded 10 %, for simplicity. More refined values of this threshold should be further investigated in the future by the authors and could be defined by regulations, considering also the uncertainty associated to the PoF. When a considered section overcomes this threshold limit after the extreme event, the command-and-control office triggers the safety teams to gather information about specifical structural elements determinant for SI assessment.

If the crew is available to gather the requested damage report, it is possible to filter the sub-damage database, giving more importance to the damage combination that occurred with higher probability, based on the crew observations. This is equivalent to filtering the sub-damage database based on the human knowledge and recomputing the entire SI analysis to obtain a refined estimation of PoF, as detailed in the following section.

3.6. Human information report

3.6.1. Types of human judgment

Given the vast size of the containership structure, the command-and-control office must guide the on-board safety teams based on the computed PoF asking specific information about the damage state of specific structural elements. In many real-case scenarios, direct access to the damaged area is often impossible for the crew due to the risks such flooding or fire. Therefore, the command-and-control office must request specific information that safety team can reliably gather from the damaged compartments. It is inefficient to inquire about structural elements that are not critical for the ship's SI. Here, since damages are simulated on the outer bottom, it is useful to ask the status about the plating, girder and floors, since they are much more decisive for the SI computation. Since an UNDEX event occurred, a specific diving team is activated by the command-and-control office to check specific structural element states. As explained in Section 3.3.1, each structural element involved in the damage can have a variable value of residual stiffness, expressed by the variable K_z. However, given the challenges of real-time

damage observation, the safety team is only required to report whether a specific element is intact or broken. The safety team must also inform the damage control office if they are not able to gather the required data.

It is essential to notice that only the status of key structural elements, such as girders, and floors, are requested for the computation of the ship's updated SI. While stiffeners were previously considered in blocks, no specific information about them is required as they are less critical for the overall SI. Consequently, it is unnecessary to gather data on all the p elements beneath the damaged panels. Instead, the crew is instructed to report the condition of a selected elements, denoted as q, which is formed by structural elements more relevant for SI only.

Hence, the q-th element's report can be expressed with the indicator D_q:

$$D_q = \begin{cases} 1 \text{ if the element is observed as intact} \\ 0 \text{ if no information is available} \\ -1 \text{ if the element is observed as broken} \end{cases}$$

This simplified reporting process ensures smoother communication between the compartment officer and the command-and-control office, minimizing the risk of misinterpretation and improving the efficiency of information flow for real-time applications.

3.6.2. Uncertainty in human judgment

Human observations are useful to filter the detailed damage database for a more accurate computation of PoF with uncertainties reduction. However, the observation by the safety teams is also affected by uncertainties. For this reason, the command-and-control office cannot deterministically trust the data gathered from the compartment's safety teams and a probabilistic approach must be implemented. Depending on the crew's assessment, each structural element is assigned a probability distribution across five potential stiffness levels identified by the variable K_z, reflecting the uncertainty associated with their observations, as resumed in Table 3.

An example of how to read the values in Table 3 is presented: suppose that the crew has reported a structural element (a floor for simplicity) within the damaged zone as broken ($D_q = -1$). This assumption leads to a high probability (70%) of the element having a residual stiffness equal to 0% and lower probabilities associated with the other residual stiffness values.

This approach allows for a flexible integration of human input into the structural analysis by accounting for uncertainty in the crew's observations and can potentially accommodate different experience levels of the crew.

Since no specific data or official guidelines were available in the literature regarding human judgment in damage assessment under emergency conditions, the probabilities in Table 3 were chosen based on reasonable assumptions, primarily to demonstrate the methodology. These values are not intended to reflect actual crew behaviour under stress. The use of assumed probabilities may lead to potential risks, such as false positives or false negatives in the damage diagnosis process, especially if the assumed distributions deviate significantly from real crew behaviour. However, the framework is designed to be flexible: the belief matrix can be readily updated when more accurate empirical data become available. Future work should prioritize empirical validation of these belief distributions, for instance through structured surveys or controlled inspection campaigns in which multiple inspectors assess the condition of damaged structural elements under realistic operational constraints. The collected observations could then be used to derive statistically meaningful human belief percentages and better represent real-world variability and uncertainty in crew assessments.

Table 3
Probability [%] associated to human believe, based on crew observation report and residual stiffness of structural elements.

		Residual stiffness of a structural element K_z				
		0%	25%	50%	75%	100%
Crew observation	*Broken* $D_q = -1$	70	15	10	3	2
	Intact $D_q = 1$	2	3	10	15	70
	Unknown $D_q = 0$	20	20	20	20	20

3.6.3. Bayes theorem applied to human judgment for the update of the damage state

Bayes' theorem is applied to update the probability distribution of damage based on the crew's observations. The goal is to combine prior knowledge with new evidence (the crew's observations) to calculate the posterior probability of each damage scenario. Bayes' theorem, in its general form, is given by [79–81]:

$$P(H|E) = \frac{P(E|H)\cdot P(H)}{P(E)} \tag{12}$$

Where $P(H)$ is the prior probability of the hypothesis H, $P(E)$ is the marginal probability of the evidence E, $P(E|H)$ represents the likelihood, or the probability of observing evidence E given that hypothesis H and finally $P(H|E)$ is the posterior probability, or the probability of hypothesis H given the evidence E. Eq. (12) represents the generic form of the Bayes' theorem, which needs to be specialized for updating the damaged state configurations. A new vector, DSR_δ, must be defined, representing the damage state report, i.e. a vector that contains the values D_q, for only structural elements that need a check by the crew. Specifically:

$$DSR_\delta = \{D_q | q = 1, \ldots, w\} \tag{13}$$

Where w is the number of structural elements requested to check by human, D_q represents the indicator of human judgment ($D_q \in \{-1, 0, +1\}$) for the q-th element, and finally δ is a sequential number that represents the number of times a report is requested from the crew (in fact, in variable contexts, such as after extinguishing a fire, a new observation may be requested to confirm or invalidate previous assessments). Given the challenging conditions under which the compartment's safety teams operate while gathering information, the process is initially simplified by focusing on the structural elements that have significant relevance to the structural integrity in the section with the highest PoF. Should the conditions allow, subsequent observations may include structural elements in sections with lower PoF, to maximize, where feasible, the advantage that human observations can provide. Based on that, Eq. (12) becomes:

$$P(DS_{ij}|DSR_\delta) = \frac{P(DSR_\delta|DS_{ij})\cdot P(DS_{ij})}{P(DSR_\delta)} \tag{14}$$

Where $P(DS_{ij}|DSR_\delta)$ is the posterior probability of the damage pattern DS_{ij} given the crew's observation DSR_δ, $P(DSR_\delta|DS_{ij})$ is the likelihood (Table 3), $P(DS_{ij})$ is the prior probability of the damage pattern (before considering the human input), and finally $P(DSR_\delta)$ is the marginal probability of the observation, typically found as a normalising constant.

With the computation of the posterior probability, is possible to update the probability of occurrence of a specific damage combination based on the human knowledge so that it is possible to recalculate the PoF merging the previous sensors and FEM data with on-board crew perception.

3.6.4. Prior definition within the Bayes approach

The computation of the prior probability $P(DS_{ij})$ within Eq. (14) can be addressed following three different approaches, presented as follow.

- The first method is the simplest, as it assumes a uniform prior, where all damage combinations are considered equally likely. In this case, the prior probability for each combination is simply the inverse of the total number of damage combinations considered.
- The second method considers an informative non-uniform prior. The non-uniform priors can be derived from the KDE distributions

obtained from Section 3.5.1. The damage combinations that generate stress value with higher probabilities, based on the KDE results, are assigned higher prior values, while those with lower probability receive lower priors.

- The third method uses the existing strain sensor network, previously employed for localization (as described in Section 3.2.1), to compute the non-uniform priors. This approach assigns higher prior values to damage combinations that, based on strain comparison, most closely match the actual damage on the structure.

The second approach is the one followed in the present investigation, as it provides a more detailed and complete representation of the actual damage scenario based on the available information.

3.6.5. Updating the probability of failure

After having computed the posterior probability for each damage combination based on human reports, the last step is updating of the PoF. As explained in Section 3.5.1, with the values of stress obtained for each damage combination and for each ship section, it is possible to generate frequency histograms. With the posterior probabilities, improvements can be done by updating those histograms setting the frequency of each stress value insert proportionally to the posterior probability of the related damage combination. In this way, the frequency histograms, from which the SI is investigated, are plotted in a more structured manner, taking into considerations the information derived from the on-board crew observations, giving more relevance to damages that, through the bayes theorem, are recognized as most likely to the real occurred damage.

As described in Section 3.5.1, histogram can be converted into continuous distributions through the KDE function, and then, comparing those stress distribution with the material yielding limit distribution, the PoF can be computed. The new calculated value of PoF is more reliable since it derived from multiple sources of information merged in a structured mathematical manner. It is also possible to demonstrate that the newly calculated PoF value is less affected by uncertainty. Since the PoF is computed based on the continuous stress distribution, Shannon entropy [82] can be employed as a measure to quantify how dispersed (high uncertainty) or concentrated (low uncertainty) the probability distribution is. The Shannon entropy H for the continuous stress distribution of a specific τ ship transversal section obtained via KDE can be calculated as follows [83,84]:

$$H_\tau = -\int f_{s\tau}(s)\cdot\log(f_{s\tau}(s))ds \tag{15}$$

Where $f_{s\tau}(s)$ represents the probability density function of the stress continuous distribution of a specific τ ship transversal section. To facilitate the interpretation of entropy values, the normalized entropy can be calculated, which compares the computed entropy with the maximum possible entropy for that distribution:

$$H_{norm,\tau} = \frac{H_\tau}{H_{max,\tau}} \tag{16}$$

Where $H_{max,\tau}$ is equal to $\log(m)$, where m represent the total number of sub-damage cases so the total number of points in the distribution. This normalized value allows for an easier assessment of uncertainty reduction, as it ranges from 0 (minimum uncertainty) to 1 (maximum uncertainty). Finally, the normalized uncertainties of the individual sections must be combined to obtain a global uncertainty that represents the entire ship. One possible strategy is to use a weighted average, which allows sections with higher probabilities of failure to contribute more significantly to the global uncertainty measure. This approach provides a more accurate reflection of the overall structural risk by emphasizing areas most likely to impact the ship's integrity.

$$H_{global} = \frac{1}{\sum\omega_\tau}\cdot\sum_{\tau=1}^{\theta}\left(\omega_\tau\cdot H_{norm,\tau}\right) \tag{17}$$

Where θ is the total number of considered transversal section (as shown in Fig. 7, in this case study θ is equal to seven), and ω_τ is a weight associated with section τ-th, proportional to its PoF, calculated as:

$$\omega_\tau = \frac{PoF_\tau}{PoF_{global}} \tag{18}$$

In this way, it is possible to assess whether the integration of human information effectively leads to PoF results that are less affected by uncertainty.

Although the present study does not report detailed computational benchmarks, it is important to highlight that the core numerical operations involved in the proposed framework—such as damage localization through pattern recognition, sub-damage database weighting, stress distribution computation, and probabilistic PoF estimation—are computationally efficient and compatible with real-time or near-real-time execution. These operations were implemented in a highly streamlined pipeline and executed within seconds on a standard workstation. However, the total response time of the framework also depends on the availability and quality of human feedback, which is inherently variable and difficult to quantify. Factors such as the crew's proximity to the damage site, environmental hazards, communication delays, and the level of crew training can introduce uncertainties and potential delays in the overall decision-making process. As a result, while the numerical framework is ready for real-time application, the integration of human observations in time-critical scenarios requires further validation through experimental trials or operational simulations to evaluate practical feasibility.

As demonstrated, to further improve computational scalability, two key strategies have been integrated into the framework. First, the use of LHS enables an efficient exploration of the damage state space with a significantly reduced number of simulations compared to full combinatorial enumeration. In the present study, convergence of the PoF estimation was observed with 1000 samples, beyond which improvements were negligible—demonstrating a favorable trade-off between computational effort and output stability. Second, an ANN surrogate model was trained offline to predict key parameters related to structural integrity and PoF. Once trained, the ANN enables near-instantaneous evaluation of new damage combinations, requiring only milliseconds per prediction. This approach ensures that the decision-support pipeline remains lightweight and responsive even when the number of damage configurations increases.

In addition, the modular structure of the framework allows users to tailor the level of model refinement depending on available computational resources or mission-specific constraints, enabling selective simplification in less critical regions. This adaptability ensures that the framework remains applicable across a wide range of structural scenarios while maintaining computational feasibility.

4. Results and discussion

The results of the framework application, as outlined in the scheme of Fig. 1, are reported and discussed below. Fig. 8 illustrates the results regarding the simulation of the UNDEX phenomenon and its effects on the structure. Specifically, Fig. 8(a) shows a section of the numerical model, highlighting the impact of the shock wave generated by the UNDEX on the structure. The field distribution of the variable POR (total dynamic acoustic pressure) is shown at the zero-time instant of the analysis. The maximum shock wave POR measured was $4.7{\cdot}10^7$ $[Pa]$, close to the values prescribed by Cole's formulation [58]. This result reinforces the reliability of the model in replicating real-word conditions. Additionally, Fig. 8(b) shows the total displacement contour of the structure at the time of the explosion was recorded, further illustrating

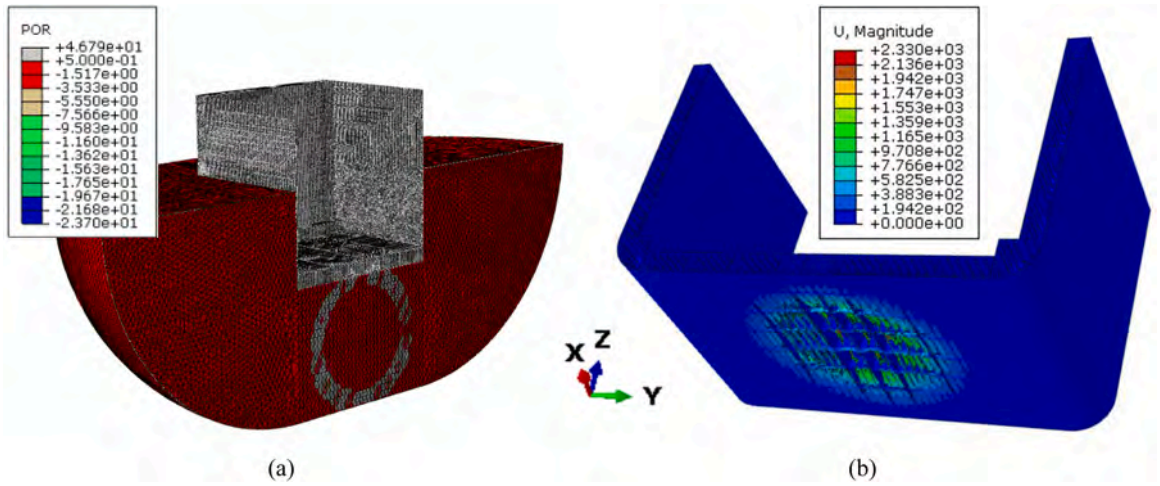

Fig. 8. (a) Computed POR field (in [MPa]) at the zero-time instant due to total wave formulation, (b) magnitude displacement contour (in [mm]) at $t = 50$ [ms] (with bulkheads shaded).

the structure's immediate response.

As mentioned earlier, a second, more simplified model was created based on the previous one to mimic the behaviour of the damaged structure. The result of applying the operational loads to this model, with simplified damage, is shown in Fig. 9(a).

The next step of the framework is to extract the strain values from these two models associated with the sensor network shown in Fig. 5(a), to perform damage localization using the initial offline database and the SSE metric. The results, in terms of normalized weight calculated based on the SSE outcomes, are presented in Fig. 9(b). The first observation, visible in Fig. 9(b), is that the pattern recognition metric can accurately localize the damage—or, more precisely, it identifies the database case most like the target (case *I*, Fig. 5(b)), for both the target models. In fact, Case *I* in the offline database has a very high normalized weight, indicating that the algorithm identified it as the most like the target damage based on strain comparison. This indicates that the use of a simplified damage model does not compromise the accuracy of the damage analysis, while offering the significant advantage of a much lower computational burden compared to a HiFi simulation.

For this reason, it was deemed appropriate to proceed with the framework implementation using the simplified target damage only.

Although the other two cases of the offline database demonstrate a lower level of similarity, especially Case *III*, they are still considered in the subsequent phases of the SI study. Despite the lower similarity, they are not completely negligible as they still show some degree of resemblance. By appropriately weighting the three cases in the database based on these results, it is possible to reasonably recreate the actual damage with minimal simplification. This approach ensures a good representation of the real damage while maintaining computational efficiency.

After completing the damage localization phase, the subsequent phase involved the creation of the sub-damage database. The creation of the sub-damage database facilitated the computation of stress values of ship's sections for each damage state DS_{ij} configuration generated through the LHS method, subsequently enhanced using an ANN.

Initially, these stresses are represented as discrete distributions (frequency histograms), which are then transformed into continuous distributions through the KDE approach. These distributions are derived from stress values obtained by applying the LHS method in combination with the ANN, as described in Section 3.3.4. This approach ensures optimal coverage of all possible damage combinations. Given that containership sections labelled as $1, 2, 6, 7$ (Fig. 7) are assumed to remain unaffected by the damage (both in the context of simplified target damage and the damage cases in the database), their corresponding stress values remain consistent with the baseline stress (which

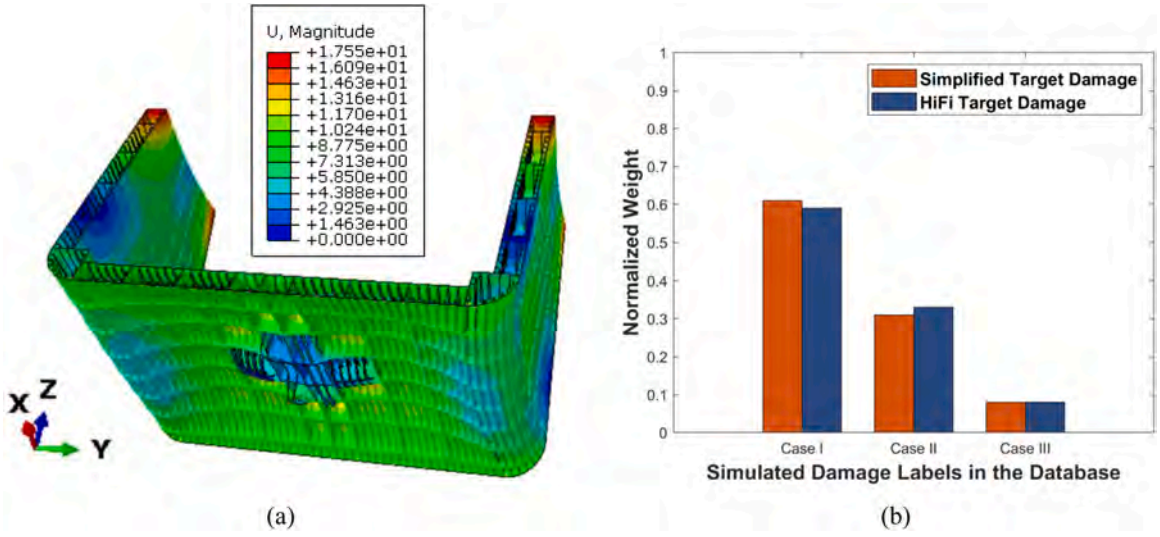

Fig. 9. (a) Displacement field of the simplified target model (in [mm] and with bulkheads shaded) and (b) normalized weight resulting from the strain comparison between the first offline database with the simplified target damage and the HiFi one.

is the design stress value). Based on that, the analysis focuses on the discrete and continuous stress distributions of the damaged sections labelled as $3,4,5$, which are illustrated in Fig. 10.

The resulting continuous stress distributions of Fig. 10 exhibit non-Gaussian characteristics, which means that they are non-symmetric and may assume irregular shapes. This behaviour arises from the inherent complexity of the damage configurations considered in the analysis, as each configuration contributes distinct and varying stress levels across the damaged sections.

Fig. 11 illustrates the stress distribution across the ship's sections, clearly delineating the differences between damaged and undamaged regions. Sections $1,2,6,7$ maintain consistent stress levels, corresponding to baseline conditions (no damage). Conversely, sections 3,4,5 exhibit elevated stress due to structural damage, and in particular Section 4 experienced the most significant increase of stress level. Fig. 11 further emphasizes the variability in post-damage stress and its proximity to the yield stress of the steel material of the ship, a critical factor in the subsequent SI assessment.

Based on the formulations presented in Section 3.5, the $\mathrm{PoF}_{\mathrm{global}}$, prior to human observations, was computed to assess how far the containership portion is from material yielding threshold. The results are resumed in Table 4. It is possible to notice that for the non-damaged sections the PoF is less than 10^{-8} which means, as stated in Paragraph 3.5.2, common design rules for containership are respected.

Considering the damaged sections, they exhibit significantly higher PoF values due to the presence of extensive structural damage induced by the UNDEX event. Notably, transversal Section 4 presents the higher PoF value equal to 0.11307. For what concern the $\mathrm{PoF}_{\mathrm{global}}$, it exceeds the critical 10% threshold (user-defined), suggesting a heightened risk of failure. As a result, the on-board crew is activated to collect detailed structural information, particularly for critical elements such as girders and floors, in the section with higher PoF (Section 4). This effort aims to reduce uncertainty and provide a more accurate PoF estimation for the damaged areas. Fig. 12 highlights the 13 structural elements in Section 4 considered the most critical for SI, and therefore, those for which information from the crew is requested.

To enhance the interpretation of results when integrating human information into the framework, two extreme scenarios are analysed along with a third case that more accurately represents a realistic case.

In the first extreme scenario, the PoF in Section 4 is updated assuming that the on-board crew reports all the significant structural elements for SI computation in that section as intact. Specifically, $DSR_{\delta} = \{D_q | D_q = 1,\ \forall q = 1,2,\ldots,13\}$. Note that, it is assumed that the on-board team can report the structural condition of all these thirteen structural elements. Fig. 13 illustrates the pre and post human information stress distributions for the first case.

From Fig. 13, it is evident that, following the information provided by the on-board crew, the stress peak shifts toward lower stress values. This is because the stress corresponding to damage combinations where the structural elements requested are identified as intact are given more

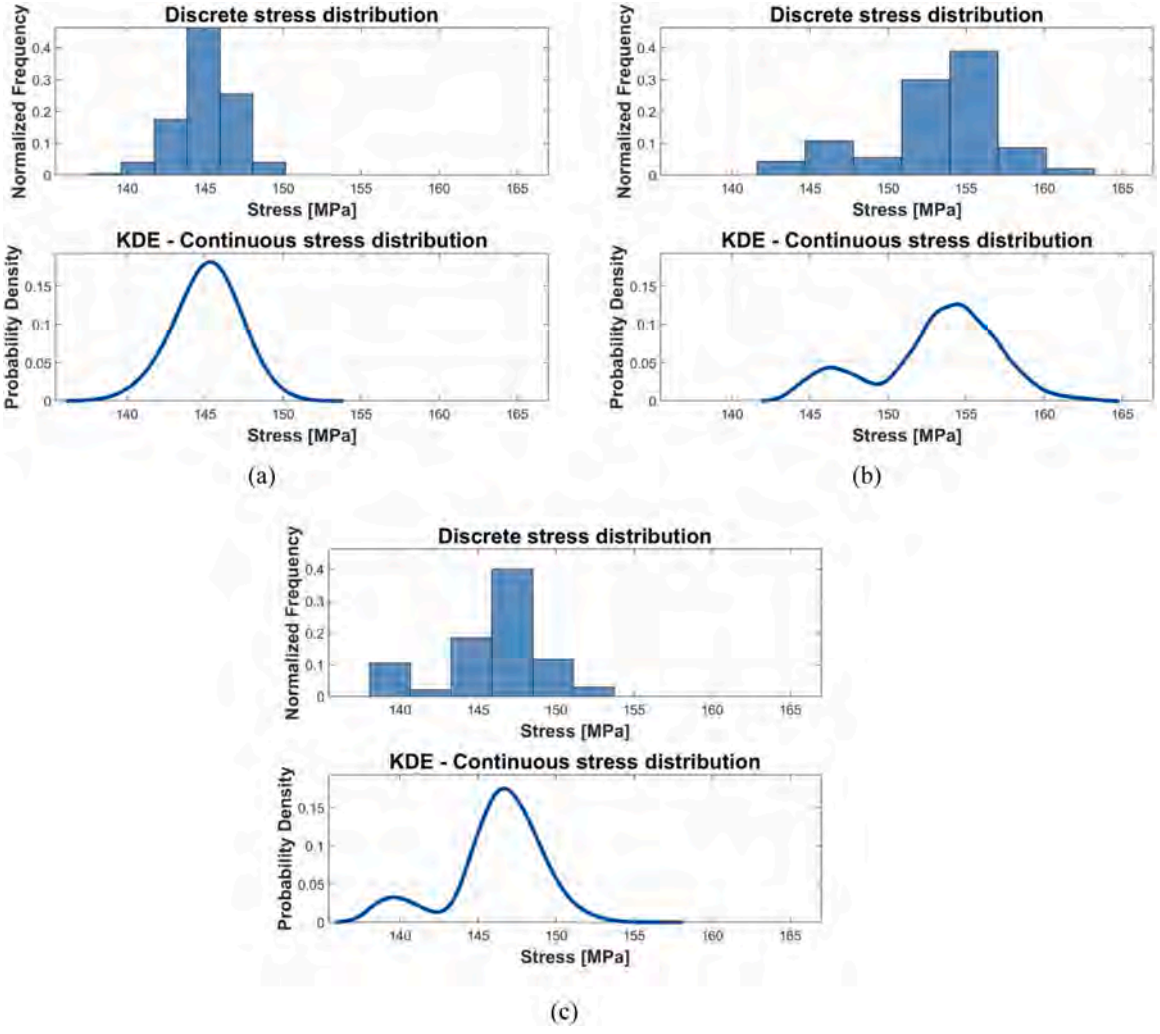

Fig. 10. Visualization of discrete and continuous maximum stress distribution for three cross-sections of the containership model: (a) Section 3, (b) Section 4 and (c) Section 5.

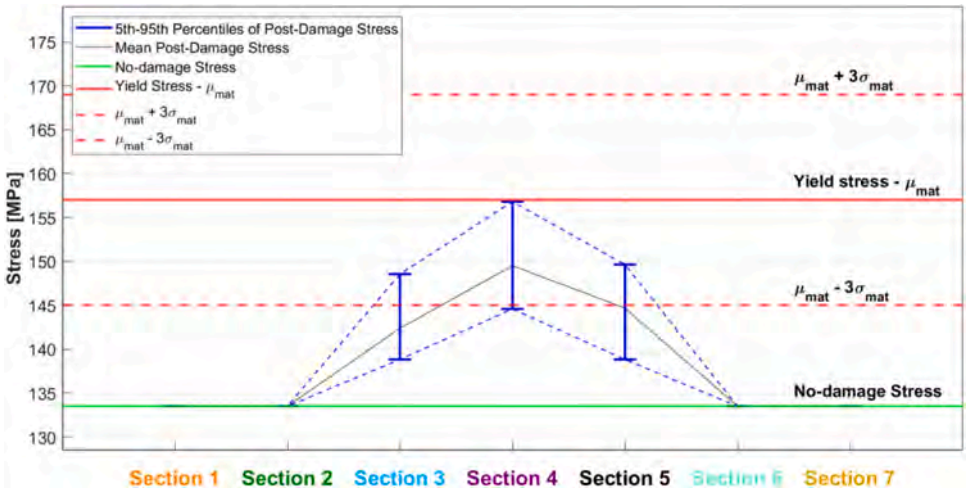

Fig. 11. Visualization of the maximum stress distribution with percentiles with respect to the yielding material limit for the seven transversal sections of the ship with reference to Fig. 7.

Table 4
PoF_{global} calculation prior to human observation.

	Section 1	Section 2	Section 3	Section 4	Section 5	Section 6	Section 7
PoF_{τ}	$5.9{\cdot}10^{-9}$	$5.9{\cdot}10^{-9}$	0.00394	0.11307	0.00880	$5.9{\cdot}10^{-9}$	$5.9{\cdot}10^{-9}$
$PoF_{global} = 1 - \prod_{\tau=1}^{\theta}(1 - PoF_{\tau}) = 0.12434$							

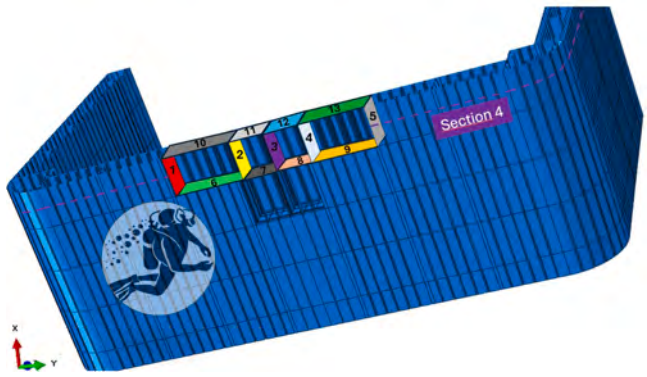

Fig. 12. Visualization of the 13 structural elements in Section 4 critical for SI for which onboard crew observation is required to update the PoF.

weight and now plays a greater role in the creation of the SI histograms. Consequently, the updated PoF for Section 4 decreases from 0.11307 to 0.04355, while the PoF_{global} reduces to 0.05570.

In the second extreme scenario, the PoF in Section 4 is updated assuming that the on-board crew reports all significant structural elements for SI computation in that section as broken. Specifically, $DSR_{\delta} = \{D_q | D_q = -1, \forall q = 1,2,\ldots,13\}$. Even here, it is assumed that the on-board team can report the structural condition of all these structural elements. Fig. 14 presents the pre and post human stress distributions for this scenario.

As expected from Fig. 14 it is evident that, following the information provided by the on-board crew, the stress peak shift toward higher stress values. This is because the stress corresponding to damage combinations where the structural elements requested are identified as broken are given more weight and now plays a greater role in the creation of the SI histograms. Consequently, the updated PoF for Section 4 rises from 0.11307 to 0.24076, while the PoF_{global} increases to 0.25726.

These two cases, although they effectively illustrate how the integration of human information leads to a more accurate PoF, are extreme scenarios. One of the strongest assumptions is that, out of the thirteen structural elements in the most damaged section, the on-board crew can provide information for all of them. For this reason, results from a third case, which more closely resembles reality, are also presented here. In this scenario, it is assumed that due to the difficulties faced by the on-board crew, they can provide the condition for only three of the elements, while for the others, the response is "unknown" ($D_q = 0$). Specifically, let's assume that $DSR_{\delta} = \{0,0,1,0,0,0,-1,0,0,0,-1,0,0\}$. Fig. 15 presents the pre and post human stress distributions for this scenario.

It is immediately noticeable that, unlike the two previous extreme cases, the variation in the stress distribution shifts towards higher values but in a less drastic manner. The result is that the updated PoF for Section 4 rises from 0.11307 to 0.14996, while the global PoF increases to 0.16038. These PoF results are consistent with the presented stress distribution graphs.

Finally, the last result that is crucial to report to validate the methodology, is the change in uncertainty regarding the PoF through Shannon entropy before and after the human observation. The results are presented in Table 5.

In all the three cases the Shannon entropy decreases, demonstrating that the new PoF values are less affected by uncertainty in the stress distribution, precisely due to the integration of human information. By incorporating human knowledge into the PoF assessment, these updated calculations provide a more reliable result, reducing uncertainties and enabling more informed real-time decision-making.

5. Conclusions

The present study addressed the critical inefficiencies in the current damage management systems on military ships, particularly in integrating sensor data with human input for real-time decision-making. The traditional reliance on manual assessments introduces significant

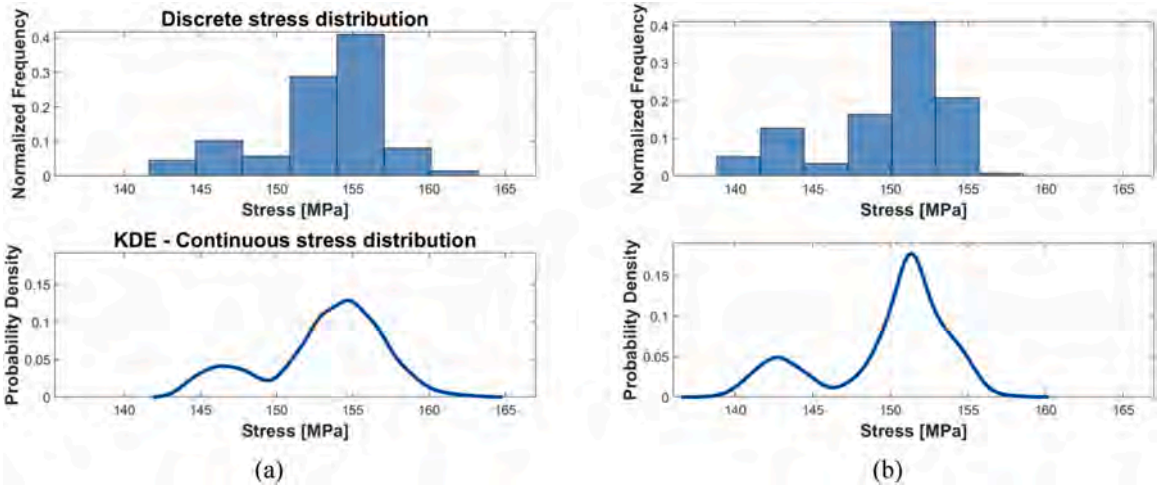

Fig. 13. Section 4 maximum stress distribution after the damage: (a) prior human information and (b) post human information.

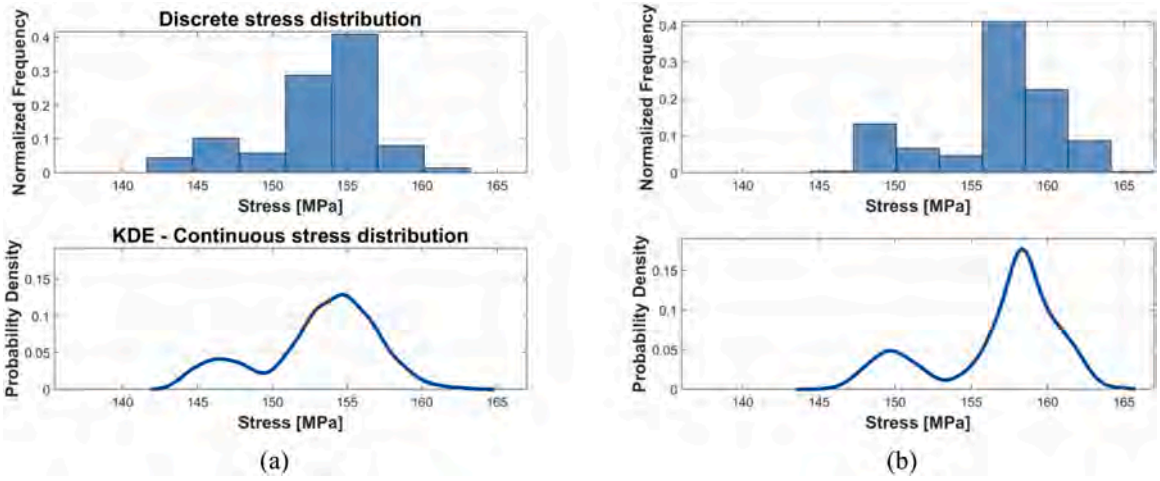

Fig. 14. Section 4 maximum stress distribution after the damage: (a) prior-human information and (b) post-human information.

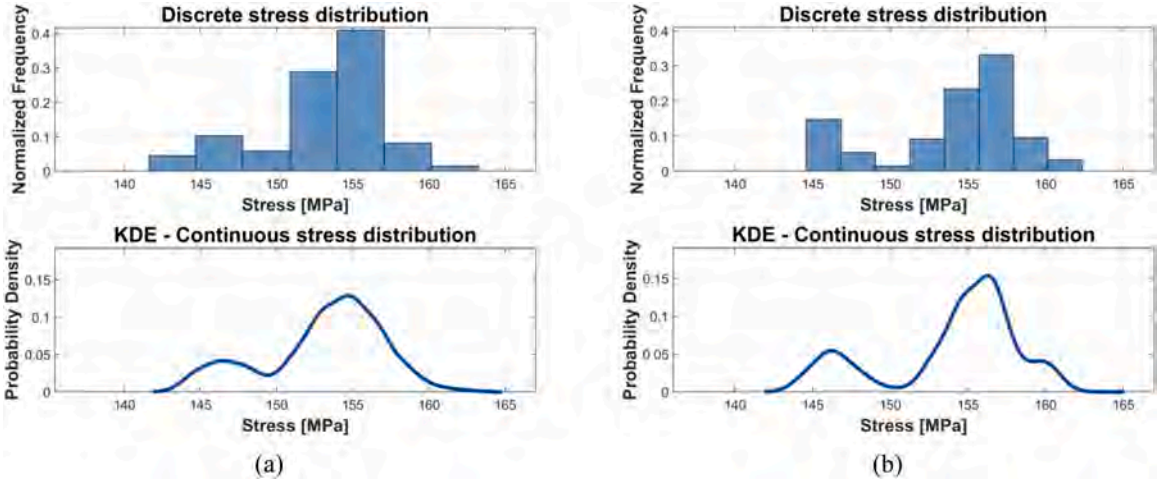

Fig. 15. Section 4 maximum stress distribution after the damage: (a) prior-human information and (b) post-human information.

delays, miscommunications, and errors, especially when rapid action is required to mitigate threats. Despite the benefits of SHM systems, their application to large, complex structures like ships remains limited by incomplete sensor coverage and the inability to accurately determine the full morphology of the damage. Furthermore, existing automated systems have not yet achieved the level of reliability required to fully replace human judgment, making the integration of human information essential.

Table 5
Pre- and post-human observation PoF uncertainty reduction.

	Pre − human	*Post − human*		
		Case 1	*Case* 2	*Case* 3
H_{global}	0.57113	0.49483	0.50563	0.54011
Percentage reduction		15%	14%	8%

To overcome these limitations, a novel probabilistic framework was developed, combining sensor data, human observations, offline numerical simulations within a probabilistic framework. This framework allows for an improved assessment of the ship's structural integrity and enhances the accuracy of real-time failure probability predictions. The methodology presented by the authors is the first to implement such a combination in a maritime context, particularly focusing on a section of a containership subjected to underwater explosion damage. The framework demonstrated the ability to localize damage using strain data and pattern recognition techniques, leveraging precomputed databases of damage scenarios. Moreover, the integration of human reports through Bayesian updating significantly reduced uncertainty in the PoF calculations, providing a more reliable assessment of the ship's condition.

The results applied to the case study confirm the validity and effectiveness of the proposed approach. The calculated PoF values for damaged sections were successfully updated based on human input, showcasing the framework's capability to refine stress distributions and PoF estimations in real time. Importantly, the use of both sensor data and human information improved the robustness of the decision-making process, optimizing the balance between operational efficiency and safety. The methodology, as demonstrated, offers a comprehensive strategy for managing damage in high-risk scenarios, significantly enhancing ship reliability during critical missions.

The proposed probabilistic framework has the potential to significantly impact future ship design, operation, and maintenance strategies. In the long term, integrating real-time sensor data with human input in a structured, uncertainty-aware framework could lead to more resilient naval platforms capable of autonomous damage detection, diagnosis, and recovery planning. The methodology could be embedded into digital twin systems for continuous monitoring and mission planning. Furthermore, the framework is adaptable to other complex engineering domains beyond naval applications, including offshore platforms, aerospace systems, and large civil infrastructure. In these contexts, where real-time decision-making under uncertainty is essential, the structured fusion of numerical, sensory, and human inputs can enhance both safety and operational effectiveness. The approach supports the gradual automation of damage control protocols, enabling a more balanced collaboration between human operators and onboard AI-based support systems.

Despite the promising results, several limitations affect the current implementation of the proposed framework. First, the method has been validated only on a numerical case study involving a simplified portion of a containership, due to the unavailability of detailed structural models for combat ships and the lack of experimental data for underwater explosion scenarios. Second, the pattern recognition process for damage localization is based solely on simulated strain data, without accounting for noise and disturbances that would typically affect real sensor measurements. Third, the assumptions related to human judgment—particularly the probability distributions associated with crew observations—are currently based on reasonable but non-validated estimates; experimental validation involving real inspection scenarios would be needed to calibrate these models (e.g., surveys or controlled inspections). Additionally, the damage morphology is simplified by removing bottom panels without accounting for more complex fracture propagation mechanisms, which could affect the accuracy of the PoF estimation. An additional limitation concerns the simplification of the underwater explosion (UNDEX) modeling, where the effects of gas bubble dynamics were intentionally neglected. This simplification was adopted to reduce the computational burden and to focus on the primary shock-induced damage. However, in real non-contact explosions, bubble pulsations can generate secondary pressure waves that may alter the damage morphology, particularly at local structural levels. This introduces an additional source of uncertainty that can affect both the pattern recognition and the PoF estimation phases of the framework. While the present study adopted a phenomenological approach to damage approximation that partially mitigates this issue, future work should include comparative studies between damage scenarios with and without bubble effects, to quantify their downstream impact on decision-making accuracy. Finally, the computational efficiency of the approach could become critical as the number of possible damage combinations grows, especially for larger structures or more refined models. These aspects will be the focus of future developments.

Finally, beyond the technical limitations, the practical implementation of the proposed framework in real operational contexts presents additional challenges. One critical aspect is the uncertainty associated with the time needed for human teams to access damaged compartments and deliver reliable reports. Such delays can severely impact the timeliness of Bayesian updating and decision-making. These delays depend on highly variable factors such as the location of the crew relative to the damage, the physical accessibility of affected areas, the presence of secondary hazards (e.g., fire, flooding), and the communication infrastructure onboard. Moreover, the effectiveness of human input strongly relies on adequate crew training in structural damage recognition and structured reporting protocols. These elements, while outside the scope of this study, are fundamental for real-world deployment and should be addressed in future research, ideally through full-scale onboard trials and crew readiness assessments to evaluate operational response time and reporting quality under stress.

This study establishes a solid foundation for future decision-making tools that combine human expertise with real-time structural monitoring in complex, safety-critical environments.

CRediT authorship contribution statement

Jacopo Bardiani: Writing – review & editing, Writing – original draft, Validation, Methodology, Investigation, Formal analysis, Data curation, Conceptualization. **Corrado Mazzolatti:** Writing – review & editing, Writing – original draft, Visualization, Validation, Methodology, Investigation, Formal analysis, Data curation, Conceptualization. **Andrea Manes:** Writing – review & editing, Supervision, Resources, Project administration, Methodology. **Claudio Sbarufatti:** Writing – review & editing, Supervision, Resources, Project administration, Methodology, Conceptualization.

Declaration of competing interest

The authors declare that they have no known competing financial interests or personal relationships that could have appeared to influence the work reported in this paper.

Acknowledgements

The author(s) disclosed receipt of the following financial support for the research, authorship, and/or publication of this article.

Data availability

The authors do not have permission to share data.

References

[1] F. Calabrese, A. Corallo, A. Margherita, A.A. Zizzari, A knowledge-based decision support system for shipboard damage control, Exp. Syst. Appl. 39 (2012) 8204–8211, https://doi.org/10.1016/j.eswa.2012.01.146.

[2] L. Cosby, Y. Lamontagne, Critical assessment of damage control system technologies. Contract Report, Defence R&D Canada, 2006.

[3] H.J. Kang, J. Choi, D. Lee, Coded shortcut key basis rapid plotting for onboard emergency responses, Mar. Technol. Soc. J. 55 (2021) 73–87, https://doi.org/10.4031/MTSJ.55.1.8.

[4] N.S. Suhaimi, M.I.M. Ahmad, M.Z. Nuawi, A.K. Ariffin, A.Z.M. Abdullah, Structural condition assessment based strain-stress behaviour for railway welded rail joint using rosette fibre Bragg grating optical sensor, Results Eng. 19 (2023) 101300, https://doi.org/10.1016/j.rineng.2023.101300.

[5] I. Faqih, R. Adiputra, A.R. Prabowo, N. Muhayat, S. Ehlers, M. Braun, Hull girder ultimate strength of bulk carrier (HGUS-BC) evaluation: structural performances subjected to true inclination conditions of stiffened panel members, Results Eng. 18 (2023) 101076, https://doi.org/10.1016/j.rineng.2023.101076.

[6] J. Bardiani, M. Giglio, A. Manes, C. Sbarufatti, Shape sensing with iFEM on a type IV pressure vessel based on experimental measurements, in: Proc. 10th Eur. Workshop Struct. Health Monit. (EWSHM 2024), June 2024, https://doi.org/10.58286/29654.

[7] J. Bardiani, A. Manes, M. Giglio, C. Sbarufatti, Shape sensing and damage identification with iFEM on a double bottom structure of a containership, in: Int. Symp. Ind. Eng. Autom., Cham, Springer Nature Switzerland, 2024, pp. 225–235, https://doi.org/10.1007/978-3-031-70462-8_22.

[8] J. Bardiani, C. Oppezzo, A. Manes, C. Sbarufatti, An inverse FEM for structural health monitoring of a containership: sensor network optimization for accurate displacement, strain, and internal force reconstruction, Sensors 25 (2025) 276, https://doi.org/10.3390/s25010276.

[9] A. Kefal, E. Oterkus, A. Tessler, J.L. Spangler, A quadrilateral inverse-shell element with drilling degrees of freedom for shape sensing and structural health monitoring, Eng. Sci. Technol. Int. J. 19 (2016) 1299–1313, https://doi.org/10.1016/j.jestch.2016.03.006.

[10] C. Baldwin, J. Kiddy, T. Salter, P. Chen, J. Niemczuk, Fiber optic structural health monitoring system: rough sea trials testing of the RV Triton, in: OCEANS'02 3, MTS/IEEE, 2002, pp. 1806–1813.

[11] S. Chen, J. Wang, C. Zhang, M. Li, N. Li, H. Wu, Y. Song, Marine structural health monitoring with optical fiber sensors: a review, Sensors 23 (2023) 1877, https://doi.org/10.3390/s23041877.

[12] R. Min, Z. Liu, L. Pereira, C. Yang, Q. Sui, C. Marques, Optical fiber sensing for marine environment and marine structural health monitoring: a review, Opt. Laser Technol. 140 (2021) 107082, https://doi.org/10.1016/j.optlastec.2021.107082.

[13] G. Wang, K. Pran, G. Sagvolden, G.B. Havsgård, A.E. Jensen, G.A. Johnson, S. T. Vohra, Ship hull structure monitoring using fibre optic sensors, Smart Mater. Struct. 10 (2001) 472, https://doi.org/10.1088/0964-1726/10/3/308.

[14] S. Li, A. Coraddu, F. Brennan, A framework for optimal sensor placement to support structural health monitoring, J. Mar. Sci. Eng. 10 (2022) 1819, https://doi.org/10.3390/jmse10121819.

[15] A. Silva-Campillo, F. Pérez-Arribas, J.C. Suárez-Bermejo, Health-monitoring systems for marine structures: a review, Sensors 23 (2023) 2099, https://doi.org/10.3390/jmse10121819.

[16] H.N. Li, L. Ren, Z.G. Jia, T.H. Yi, D.S. Li, State-of-the-art in structural health monitoring of large and complex civil infrastructures, J. Civ. Struct. Health Monit. 6 (2016) 3–16, https://doi.org/10.1007/s13349-015-0108-9.

[17] C. Emmanouilidis, P. Pistofidis, A. Fournaris, M. Bevilacqua, I. Durazo-Cardenas, P. N. Botsaris, A.G. Starr, Context-based and human-centred information fusion in diagnostics, IFAC-Pap. Online 49 (2016) 220–225, https://doi.org/10.1016/j.ifacol.2016.11.038.

[18] J.T. Bernardo, A methodology for hard/soft information fusion in the condition monitoring of aircraft, Multisens. Multisource Inf. Fus. Archit. Algorithms Appl. 8756 (2013) (2013) 58–71, https://doi.org/10.1117/12.2016050. SPIE.

[19] A.A. Amin, T. Alsuwian, A. Shahid, S. Waseem, Health index degradation prediction of induction motor using deep neural network algorithm, Results Eng. (2025) 104357, https://doi.org/10.1016/j.rineng.2025.104357.

[20] N. Abdulazeem, Y. Hu, Human factors considerations for quantifiable human states in physical human–robot interaction: a literature review, Sensors 23 (2023) 7381, https://doi.org/10.3390/s23177381.

[21] M.N. Chowdhury, S. Shafi, M. Arzaman, A. Farhan, B.A. Teoh, K.A. Kadhim, A.N. S. Xuan, Navigating human factors in maritime safety: a review of risks and improvements in engine rooms of ocean-going vessels, Int. J. Saf. Secur. Eng. 14 (2024), https://doi.org/10.18280/ijsse.140101.

[22] C. Dominguez-Péry, L.N.R. Vuddaraju, I. Corbett-Etchevers, R. Tassabehji, Reducing maritime accidents in ships by tackling human error: a bibliometric review and research agenda, J. Shipp. Trade 6 (2021) 1–32, https://doi.org/10.1186/s41072-021-00098-y.

[23] L.A. Derdowski, G.E. Mathisen, Psychosocial factors and safety in high-risk industries: a systematic literature review, Saf. Sci. 157 (2023) 105948, https://doi.org/10.1016/j.ssci.2022.105948.

[24] Y. Luo, X. Yang, X. Li, Z. Chen, F. Liu, Human emergency behaviour and psychological stress characteristic mining based on large-scale emergencies, Comput. Math. Organ. Theory 30 (4) (2024) 293–320, https://doi.org/10.1007/s10588-024-09384-z.

[25] D. McDonnell, N. Balfe, L. Pratto, G.E. O'Donnell, Predicting the unpredictable: consideration of human and organisational factors in maintenance prognostics, J. Loss Prev. Process Ind. 54 (2018) 131–145, https://doi.org/10.1016/j.jlp.2018.03.008.

[26] R. Lima, R. Sampaio, What is uncertainty quantification? J. Braz. Soc. Mech. Sci. Eng. 40 (2018) 1–8, https://doi.org/10.1007/S40430-018-1079-7.

[27] F. Lorenzoni, F. Casarin, M. Caldon, K. Islami, C. Modena, Uncertainty quantification in structural health monitoring: applications on cultural heritage buildings, Mech. Syst. Signal Process. 66 (2016) 268–281, https://doi.org/10.1016/j.ymssp.2015.04.032.

[28] L.D. Avendaño-Valencia, Sequential bayesian updating of local LPV models for structural damage detection under changing environment, Mech. Syst. Signal Process. 234 (2025) 112775, https://doi.org/10.1016/j.ymssp.2025.112775.

[29] A.S. Martínez, Á. Rózsás, I. Rocha, F. van der Meer, Towards practical Bayesian system identification of engineering structures with spatially dense measurements, Eng. Struct. 334 (2025) 120214, https://doi.org/10.1016/j.engstruct.2025.120214.

[30] Y. He, T. Yin, X. Wang, Design of multi-hidden-layer bayesian neural networks for model updating, Adv. Struct. Eng. 28 (5) (2025) 952–972, https://doi.org/10.1177/13694332241298020.

[31] R.P. Kiran, A. Das, S. Bansal, A state-of-the-art review of Bayesian finite element model updating techniques for structural systems, Probabil. Eng. Mech. (2025) 103761, https://doi.org/10.1016/j.probengmech.2025.103761.

[32] L. Luo, M. Song, Y. Li, L. Sun, A hierarchical Bayesian model updating method for bridge structures by fusing multi-source information, Struct. Health Monit. 24 (2) (2025) 1292–1310, https://doi.org/10.1177/14759217241253361.

[33] N. Dierksen, B. Hofmeister, C. Hübler, The Bayesian pattern search, a deterministic acceleration of Bayesian model updating in structural health monitoring, Mech. Syst. Signal Process. 225 (2025) 112259, https://doi.org/10.1016/j.ymssp.2024.112259.

[34] E.T. Uzun, Ç. Hızal, E. Aktaş, Reliability assessment of structures with bayesian model updating accelerated via polynomial-chaos-kriging metamodeling, Struct. Infrastruct. Eng. (2025) 1–22, https://doi.org/10.1080/15732479.2025.2474115.

[35] G. Qu, L. Sun, Performance prediction for steel bridges using SHM data and bayesian dynamic regression linear model: a novel approach, J. Bridge Eng. 29 (7) (2024) 04024044, https://doi.org/10.1061/JBENF2.BEENG-6435.

[36] M. Grootjen, M.A. Neerincx, J.A. Veltman, Cognitive task load in a naval ship control centre: from identification to prediction, Ergonomics 49 (2006) 1238–1264, https://doi.org/10.1080/00140130600612705.

[37] A.A. Broer, R. Benedictus, D. Zarouchas, The need for multi-sensor data fusion in structural health monitoring of composite aircraft structures, Aerospace 9 (2022) 183, https://doi.org/10.3390/aerospace9040183.

[38] P. Wei, C. Li, Z. Jiang, D. Wang, Real-time digital twin of ship structure deformation field based on the inverse finite element method, J. Mar. Sci. Eng. 12 (2024) 257, https://doi.org/10.3390/jmse12020257.

[39] A.J. Hughes, R.J. Barthorpe, N. Dervilis, C.R. Farrar, K. Worden, A probabilistic risk-based decision framework for structural health monitoring, Mech. Syst. Signal Process. 150 (2021) 107339, https://doi.org/10.1016/j.ymssp.2020.107339.

[40] J.A. Hiltz, Damage control and optimized manning. Tech. Rep., DRDC-Atlantic, 2005.

[41] E. Runnerstrom, Human systems integration and shipboard damage control, Nav. Eng. J. 115 (2003) 71–80, https://doi.org/10.1111/j.1559-3584.2003.tb00244.x.

[42] Lloyd's Register, Rules and Regulations For the Classification of Naval Ships, Lloyd's Register, 2005.

[43] G.I. Aravanis, N.E. Silionis, K.N. Anyfantis, Damage detection in ship hull structures under operational variability through strain sensing, Ocean Eng. 286 (2023) 115537, https://doi.org/10.1016/j.oceaneng.2023.115537.

[44] A. Pintilie, M.G. Manea, D. Mărăşescu, O. Cristea, P. Burlacu, C.P. Clinci, N.S. Popa, Optimization of bulk carrier hull design through CAD modelling and FEM structural analysis – a case study, Results Eng. 26 (2025) 104846, https://doi.org/10.1016/j.rineng.2025.104846.

[45] Smith M., ABAQUS/Standard user's manual, version 6.9, (2009).

[46] K. Alam, H. Ullah, M. Iqbal, A. Husain, A. Rasul, M. Iqbal, Structural integrity of offshore wind turbine blade under extreme gust and normal operating conditions, Results Eng. 25 (2025) 104572, https://doi.org/10.1016/j.rineng.2025.104572.

[47] A.R. Prabowo, R. Ridwan, T. Tuswan, J.M. Sohn, E. Surojo, F. Imaduddin, Effect of the selected parameters in idealizing material failures under tensile loads: benchmarks for damage analysis on thin-walled structures, Curved Layer. Struct. 9 (2022) 258–285, https://doi.org/10.1515/cls-2022-0021.

[48] S. Ehlers, J. Broekhuijsen, H.S. Alsos, F. Biehl, K. Tabri, Simulating the collision response of ship side structures: a failure criteria benchmark study, Int. Shipbuild. Progr. 55 (2008) 127–144, https://doi.org/10.3233/ISP-2008-0042.

[49] G.R. Johnson, A constitutive model and data for metals subjected to large strains, high strain rates and high temperatures, in: Proc. 7th Int. Symp. Ballistics, The Hague, Netherlands, 1983.

[50] L. Lin, X.D. Zhi, F. Fan, S.J. Meng, J.J. Su, Determination of parameters of Johnson–Cook models of Q235B steel, J. Vib. Shock 33 (2014) 153–158, https://doi.org/10.13465/j.cnki.jvs.2014.09.028.

[51] B.C. Simonsen, R. Törnqvist, Experimental and numerical modelling of ductile crack propagation in large-scale shell structures, Mar. Struct. 17 (2004) 1–27, https://doi.org/10.1016/j.marstruc.2004.03.004.

[52] J.R. Rice, D.M. Tracey, On the ductile enlargement of voids in triaxial stress fields, J. Mech. Phys. Solids 17 (1969) 201–217.

[53] Z. Tokmechi, A. Davoudi-Kia, Investigation of the probability of RCC dams' failure due to the blast loading by using the Monte Carlo method, Results Eng. (2025) 105293, https://doi.org/10.1016/j.rineng.2025.105293.

[54] Q.L. Zhang, X.Y. Huang, Z. Li, Coupled acoustic-structural analysis of a partially submerged circular RC column in an underwater explosion event: factors to be

considered for loading, Ocean Eng. 232 (2021) 109122, https://doi.org/10.1016/j.oceaneng.2021.109122.
[55] Y.S. Shin, Ship shock modeling and simulation for far-field underwater explosion, Comput. Struct. 82 (2004) 2211–2219, https://doi.org/10.1016/j.compstruc.2004.03.075.
[56] Y. Wang, H. Dong, T. Dong, X. Xu, Dumbbell-shaped damage effect of closed cylindrical shell subjected to far-field side-on underwater explosion shock wave, J. Mar. Sci. Eng. 10 (2022) 1874, https://doi.org/10.3390/jmse10121874.
[57] J. Qiankun, D. Gangyi, A finite element analysis of ship sections subjected to underwater explosion, Int. J. Impact Eng. 38 (2011) 558–566, https://doi.org/10.1016/j.ijimpeng.2010.11.005.
[58] R.H. Cole, R. Weller, Underwater explosions, Phys. Today 1 (1948) 35.
[59] C.H. Jang, D.K. Kim, An advanced technique to adjust hull girder load: part 2 – Application to ship's hull for verification, Results Eng. (2025), https://doi.org/10.1016/j.rineng.2025.104313.
[60] C.M. Salazar-Domínguez, J. Hernández-Hernández, E.D. Rosas-Huerta, G.E. Iturbe-Rosas, A.L. Herrera-May, Structural analysis of a barge midship section considering the still water and wave load effects, J. Mar. Sci. Eng. 9 (2021) 99, https://doi.org/10.3390/jmse9010099.
[61] IACS, Common Structural Rules For Bulk Carriers and Oil Tankers, Int. Assoc. Classif. Soc, 2014.
[62] M. Bonopera, Fiber-Bragg-grating-based displacement sensors: review of recent advances, Materials 15 (2022) 5561, https://doi.org/10.3390/ma15165561.
[63] D. Kinet, P. Mégret, K.W. Goossen, L. Qiu, D. Heider, C. Caucheteur, Fiber Bragg grating sensors toward structural health monitoring in composite materials: challenges and solutions, Sensors 14 (2014) 7394–7419, https://doi.org/10.3390/s140407394.
[64] S. Lee, J.W. Park, D.S. Kim, I. Jeon, D.C. Baek, Anomaly detection of tripod shafts using modified Mahalanobis distance, J. Mech. Sci. Technol. 32 (2018) 2473–2478, https://doi.org/10.3390/s24154855.
[65] P. Borisut, A. Nuchitprasittichai, Adaptive Latin hypercube sampling for a surrogate-based optimization with artificial neural network, Processes 11 (2023) 3232, https://doi.org/10.3390/pr11113232.
[66] L. Chu, E.S. De Cursi, A. El Hami, M. Eid, Application of Latin hypercube sampling based kriging surrogate models in reliability assessment, Sci. J. Appl. Math. Stat. 3 (2015) 263–274, https://doi.org/10.11648/j.sjams.20150306.16.
[67] P. Phromphan, J. Suvisuthikasame, M. Kaewmongkol, W. Chanpichitwanich, S. Sleesongsom, A new Latin hypercube sampling with maximum diversity factor for reliability-based design optimization of HLM, Symmetry 16 (2024) 901, https://doi.org/10.3390/sym16070901.
[68] J. Bardiani, L. Lomazzi, C. Sbarufatti, A. Manes, A machine learning-based tool to correlate coupled and uncoupled numerical simulations for submerged plates subjected to underwater explosions, J. Marine Sci. Appl. (2025) 1–20, https://doi.org/10.1007/s11804-025-00624-5.
[69] Z. Pei, B. Yang, G. Liu, W. Wu, Experimental research on the stiffness step between the main hull and superstructure of cruise ships, J. Mar. Sci. Eng. 11 (2023) 1264, https://doi.org/10.3390/jmse11071264.
[70] O. Melnyk, S. Onyshchenko, O. Onishchenko, O. Shibaev, Y. Volyanskaya, A comprehensive approach to structural integrity analysis and maintenance strategy for ship's hull, J. Marit. Res. 21 (2024) 36–44, https://doi.org/10.1007/978-3-031-82027-4_11.
[71] Y.C. Chen, A tutorial on kernel density estimation and recent advances, Biostat. Epidemiol. 1 (2017) 161–187, https://doi.org/10.1080/24709360.2017.1396742.
[72] Bahamas Maritime Authority, Report of the investigation into the sinking of the "MOL Comfort" in the Indian Ocean. The Commonwealth of the Bahamas, 2015.
[73] S.Z.A. Syed Ahmad, M.K. Abu Husain, N.I. Mohd Zaki, N.A. Mukhlas, E. Mat Soom, N.U. Azman, G. Najafian, Offshore structural reliability assessment by probabilistic procedures—A review, J. Mar. Sci. Eng. 9 (2021) 998, https://doi.org/10.3390/jmse9090998.
[74] O. Ditlevsen, H.O. Madsen, Structural Reliability Methods, Vol. 178, Wiley, New York, 1996.
[75] R.E. Melchers, A.T. Beck, Structural Reliability Analysis and Prediction, John Wiley & Sons, 2018.
[76] K. Tabri, H. Naar, M. Kõrgesaar, Ultimate strength of ship hull girder with grounding damage, Ships Offshore Struct. 15 (Suppl. 1) (2020) S161–S175, https://doi.org/10.1080/17445302.2020.1827631.
[77] A. Prestileo, E. Rizzuto, A.P. Teixeira, C.G. Soares, Bottom damage scenarios for the hull girder structural assessment, Mar. Struct. 33 (2013) 33–55, https://doi.org/10.1016/j.marstruc.2013.04.001.
[78] A.W. Hussein, C.G. Soares, Reliability and residual strength of double hull tankers designed according to the new IACS common structural rules, Ocean Eng. 36 (17–18) (2009) 1446–1459, https://doi.org/10.1016/j.oceaneng.2009.04.006.
[79] Y. Ding, X.W. Ye, Y. Guo, R. Zhang, Z. Ma, Probabilistic method for wind speed prediction and statistics distribution inference based on SHM data-driven, Probabilist. Eng. Mech. 73 (2023) 103475, https://doi.org/10.1016/j.probengmech.2023.103475.
[80] N. Stylianides, E. Kontou, Bayes theorem and its recent applications, Math. Res. J. 2 (2020) 1–7.
[81] L.P.S. Ferreira, R. Teloli, S. da Silva, E. Figueiredo, N. Maia, et al., Bayesian data-driven framework for structural health monitoring of composite structures under limited experimental data, Struct. Health Monit. https://doi.org/10.1177/14759217241236801.
[82] C.E. Shannon, A mathematical theory of communication, Bell Syst. Tech. J. 27 (1948) 379–423, https://doi.org/10.1002/j.1538-7305.1948.tb01338.x.
[83] A. Feutrill, M. Roughan, A review of Shannon and differential entropy rate estimation, Entropy 23 (2021) 1046, https://doi.org/10.3390/e23081046.
[84] S. Robin, L. Scrucca, Mixture-based estimation of entropy, Comput. Stat. Data Anal. 177 (2023) 107582, https://doi.org/10.1016/j.csda.2022.107582.